6
Microfluidic Flows of Viscoelastic Fluids

Mónica S. N. Oliveira, Manuel A. Alves, and Fernando T. Pinho

6.1
Introduction

6.1.1
Objectives and Organization of the Chapter

In this chapter we provide an overview of viscoelastic fluid flow at the microscale. We briefly review the rheology of these nonlinear fluids and assess its implications on the flow behavior. In particular, we discuss the appearance of viscoelastic instabilities, which are seen to occur even under creeping flow conditions. The first type of instability changes the flow type from symmetric to asymmetric, while the flow remains steady. The second (and more frequent) type of instability, which sets in when elastic effects are enhanced, causes the flow to become unsteady varying in time periodically. This unsteadiness results in a nearly chaotic flow, bringing about a significant improvement in mixing performance.

After a brief introduction to the theme of microfluidics, its basic principles, relevance and applications, this chapter is organized in five additional sections. Section 6.2 provides an overview of the problem of mixing at the microscale and of the current methods used to tackle this problem. Section 6.3 presents an introduction to non-Newtonian viscoelastic fluids describing their most relevant rheological properties. Section 6.4 presents the governing equations for Newtonian and non-Newtonian fluid flow, including the constitutive equations that describe the rheology of the fluids. Section 6.5 deals with passive mixing methods in viscoelastic fluid flows, whereas in Section 6.6 other forcing methods for promoting viscoelastic fluid flow at the microscale are briefly described.

6.1.2
Microfluidics

6.1.2.1 Basic Principles, Relevance, and Applications

Microfluidics is a technological field that deals with the flow and handling of fluids in submillimeter-sized systems. Common microfluidic systems have features (typically

Transport and Mixing in Laminar Flows: From Microfluidics to Oceanic Currents,
First Edition. Edited by Roman Grigoriev.

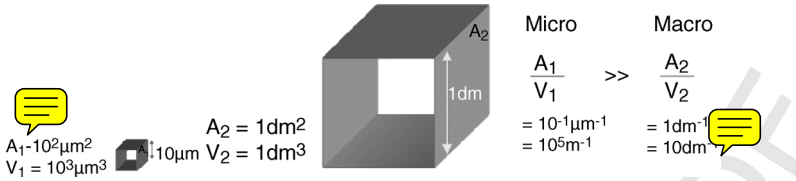

Figure 6.1 Surface-to-volume ratio: from macro- to microscale.

the channel width) with characteristic dimensions on the order of 10s to 100s of microns [1, 2]. The depth of the channels is usually of the same order of magnitude (~10–100 µm), while channel lengths may be much larger (up to ~500× the width, that is, 5–50 mm long).

One key benefit of miniaturization is the dramatic reduction in the required fluid sample volume: a linear reduction in the characteristic dimension of the device (L) by a factor of 10^3 (e.g., from 1 cm to 10 µm) amounts to a volume reduction by a factor of 10^9 (L^3). In microfluidic devices, the sample volumes required to fill up a channel typically range from the microliter scale down to the nanoliter scale. Furthermore, as a consequence of miniaturization, high surface-to-volume ratios are observed in microfluidic devices, as illustrated in Figure 6.1.

The high surface-to-volume ratios typical of microfluidics imply that the balance between surface forces (e.g., due to viscous friction and surface tension) and volume forces (e.g., inertia, gravity) is shifted toward the former. This represents a major difference relative to macroscale flows, and is crucial for several practical applications. For example, it is possible to fill up a microchannel by capillarity, which would be unthinkable in a macro device – this principle is commonly used in commercial systems, such as glucose and cholesterol meters to lead the blood droplet through the capillary in the test strip where a chemical reaction takes place.

Both macro- and microfluidic flows are commonly driven by pressure gradients and these are frequently induced using pumps. In microfluidics, special positive displacement pumps, such as syringe pumps, are typically employed to pump the fluid through the device. Alternatively, electro-osmosis (EO) can be used to drive and control liquid flows, provided the fluid contains electrolytes. Electrokinetic flows have been used for a long time in colloidal and porous systems [3, 4], but have only really come of age in microfluidics. The formation of an electric double layer (EDL) allows electrically conductive fluids to be moved in the microchannels by EO (e.g., [5, 6]). The microchannel walls (as most solid surfaces) acquire an electric charge when in contact with an electrolyte (e.g., water) – an EDL of counter-ions will form spontaneously at the walls by attracting nearby counter-ions and repelling co-ions. When an electric potential is applied across the channel, the ions in the EDL move in the direction of the electrode of opposite polarity. This causes a motion of the fluid near the walls, which in turn creates an advective motion of the bulk fluid through viscous forces. The fluid motion exhibits a plug-like profile instead of the characteristic parabolic velocity profile of pressure-driven flows (PDF). Once more, Electro-osmotic flows (EOF) are effective at the microscale because of the dominance of surface effects relative to volume effects. In addition to EO, there are other electrokinetic

effects important at the microscale, namely electrophoresis, sedimentation potential, and streaming potential. These concepts are thoroughly reviewed by Bruus [6] and there are many other interesting references and reviews available for electrokinetic effects in microfluidic devices (e.g., [7–11]).

The relative balance between inertial and viscous forces is normally quantified in terms of the dimensionless Reynolds number, defined as

$$\mathrm{Re} = \frac{\varrho UL}{\eta} \tag{6.1}$$

where L is a characteristic dimension of the channel, U is a characteristic velocity, usually the average velocity, and ϱ and η are the density and shear viscosity of the fluid, respectively. The magnitude of the Reynolds number is useful to identify the flow regime – laminar or turbulent. The reduced length scales and the dominance of viscous forces over inertial forces means that the flows in microfluidic channels are typically characterized by low to moderate Reynolds numbers (usually smaller than 100, and often smaller than 1). At these low Reynolds numbers, the flow is laminar and no turbulence occurs in contrast to what is usually found at the macroscale. Indeed, for laminar flow to be achieved at the macroscale, highly viscous fluids or very low velocities must be employed, whereas at the microscale, laminar flows can be readily achieved even with low viscosity fluids such as water. This is a major change relative to classical transport processes at the macroscale, and may be an advantage or a disadvantage, depending on the particular application in mind. A number of new technological applications have emerged to take advantage of the laminar behavior of the flow, such as bioassays [12, 13], sorting and separating products of a reaction [1], or microfabrication using UV laminar flow patterning [14]. Conversely, many applications require intense mixing, which can be easily (and rapidly) achieved at the macroscale as fluids mix advectively under high inertia flow conditions, but not so at the microscale where mixing relies mainly on diffusion. Nevertheless, even at Reynolds numbers below 100 it is possible to enhance mixing on the basis of momentum phenomena such as flow separation as well as viscoelastic flow instabilities [15]. The latter will be further discussed in this chapter.

Microfluidic systems have a number of other characteristics that can act as advantages or challenges depending on the application. For instance, a small consumption of reagents can be translated into significant savings both in terms of cost and time. This is critical for many applications, namely in biotechnology, when the samples to be used are costly or available only in limited amounts (e.g., blood), or when a large number of samples are needed, for example, in high-throughput screening [16]. Conversely, in applications that involve the detection of biomolecules, as the volumes are reduced, the detection signals become weaker and consequently new detection methods (and improved labels when appropriate) need to be developed for use at the microscale [17]. Furthermore, as the volume-to-surface ratio decreases, liquid evaporation can become an issue if the processes are slow and occur at high temperatures. Other advantages that arise as a consequence of the reduced length scales include significant waste reduction; reduced cost of fabrication; and possibility of producing highly integrated, disposable, and portable devices. The portability

of microfluidic devices results from a combination of the small sizes involved and the low energy consumptions, which makes this technology suitable for wireless solutions [18]. On the other hand, one of the main problems in microfluidics is that the design and fabrication of components are technologically challenging and in most cases cannot simply rely on a scaled down version of their macroscale counterparts [15]. The effort spent in developing efficient microcomponents is well apparent in the number of publications dedicated to development of micropumps, micromixers, and so on (cf. reviews [10, 19, 20] and references therein). Like component design, other difficulties in dealing with microfluidic systems are often a consequence of its youth and can potentially be overcome by further research and development. Figure 6.2 summarizes the main characteristics of microfluidic systems as well as the resulting opportunities and challenges associated with fluidic miniaturization.

The advantages identified, together with recent developments in microfabrication techniques that allow for inexpensive and rapid manufacture of high-quality geometries with well-defined micron-sized features [21–23], have stimulated a remarkable

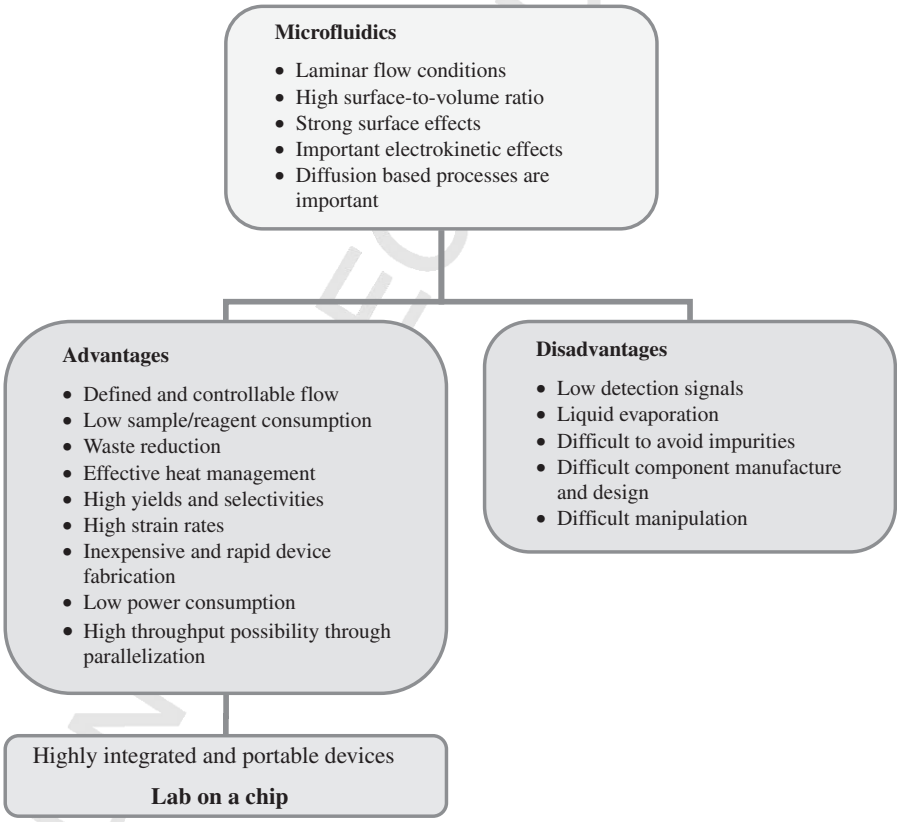

Figure 6.2 Fluidic miniaturization: opportunities and challenges.

growth and found an extensive range of applications in science and technology, as in biology, medicine, and engineering [24]. The printing heads of inkjet printers are one of the most mature commercial applications using microfluidic based systems [25]. Other examples include miniaturized systems for production of suspensions and emulsions [26, 27], immunoassays [13, 28], detection of drugs, flow cytometry [29, 30], dynamic cell separation [31, 32], cell/protein patterning [33], single cell analysis [34], manipulation and analysis of DNA molecules [35–38], and fuel cells [39]. Many other applications have been envisioned and the reader is referred to the literature for further details (e.g., [1, 9, 40, 41]).

The commercial impact of microfluidics is becoming increasingly significant and microfluidic research aspires to have an impact in the automation of biology and chemistry comparable to the microchip in electronics [1, 42]. Considering only applications in the areas of life sciences and *in-vitro* diagnostics, the market value reached 500 million Euros in 2008, and is projected to exceed 2000 million Euros in 2014 [43]. More importantly, it is anticipated that the unique characteristics of microfluidic systems have the potential to trigger a range of novel applications in many areas of science and technology [24]. One of the greatest envisaged microfluidic technological applications consists of a miniaturized laboratory where multiple processes can be integrated into a portable platform known as a lab-on-a-chip. Ultimately, this would correspond to shrinking a full production plant or an analysis laboratory into a small chip [44].

6.1.2.2 Complex Fluids in Microfluidic Flows

Many of the applications mentioned in the previous section involve handling fluids that have a complex microstructure such as polymeric solutions, whole blood or protein solutions. The flow of these fluids may prompt non-Newtonian behavior and in particular viscoelasticity [45, 46]. For instance, fluids with large polymeric molecules often exhibit elastic behavior due to the stretching and coiling of the polymeric chains, which significantly enrich flow behavior [45]. For the characterization of flows with viscoelastic fluids, in addition to the Reynolds number it is important to quantify the Deborah number, *De*, the Weissenberg number, *Wi*, and the Elasticity number, *El*. The Deborah number is defined as the ratio between the relaxation time of the fluid (λ) and the time of observation of the flow (t_f), like the duration of the unsteady part of a flow:

$$De = \lambda / t_f \tag{6.2}$$

The Weissenberg is defined as the product of the relaxation time and a characteristic rate of deformation of the flow (U/L), and quantifies the nonlinear response of the fluid

$$Wi = \lambda U / L \tag{6.3}$$

while *El* represents the ratio between elastic and inertial effects

$$El = \frac{Wi}{\mathrm{Re}} = \frac{\lambda \eta}{\varrho L^2} \tag{6.4}$$

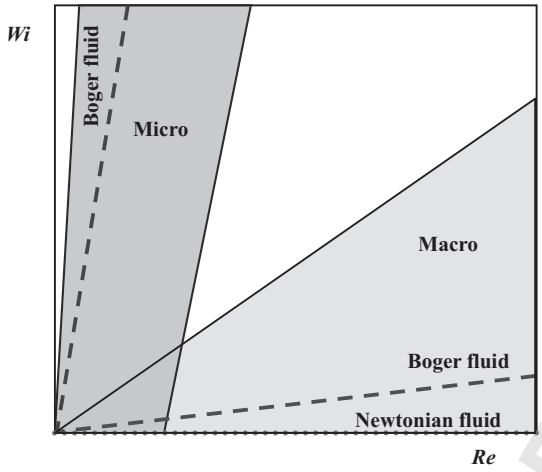

Figure 6.3 Operational regions in the *Wi*–*Re* parameter space. The dotted line corresponds to Newtonian fluids ($Wi = 0$) and the dashed lines represent a Boger fluid (i.e., viscoelastic fluid with constant viscosity, cf. Section 6.3) with low viscosity and low relaxation time in flows at the micro- and macroscale.

In steady Eulerian flows with unsteady Lagrangian characteristics, such as the flow in a contraction, the Weissenberg and Deborah numbers are proportional and, as pointed out by Dealy [47], there has been widespread misapplication of both dimensionless numbers. The small length scales together with the high deformation rates and short transit times characteristic of microfluidic systems enable the generation of high Deborah or Weissenberg number flows while keeping the Reynolds number low, leading to high *El* flows. These distinctive flow conditions result in the ability to promote strong viscoelastic effects, which are not masked by fluid inertia, even in low viscosity/elasticity fluids that would in contrast exhibit Newtonian-like behavior at the equivalent macroscale [48–52]. The dimensionless *Wi*–*Re* parameter space is depicted in Figure 6.3, where the operation regions for macro- and microscale flows are distinguished. It is clear that the geometric scale of microfluidic devices results in flows that are distinct from those seen at the macroscale, particularly when they are extension dominated [48, 49, 52–55].

6.1.2.3 Continuum Approximation

We end this introduction by analyzing the validity of the continuum approximation for modeling fluid flow at the microscale. The continuum approximation implies that fluid and flow properties (such as density, viscosity, velocity, stresses, etc.) are defined everywhere in space and vary continuously throughout space [56]. Flows can be modeled by the continuum approximation, also using molecular dynamics, which considers a collection of individual interacting molecules, or more recently as a combination of both approaches using multiscale techniques [57, 58]. Adopting the continuum approach is generally much simpler, it easily considers large systems and

is less time consuming than the other techniques, which are still not feasible for many realistic applications and for a sufficiently large number of molecules [42]. However, in simplified terms, for the continuum approximation to hold two main conditions need to be met: (i) the molecules need to be small enough compared to the characteristic length scale of the flow; (ii) the number of molecules inside each fluid element needs to be large enough. In classical fluid mechanics at the macroscale, these conditions are generally satisfied and the continuum approach generally holds [56].

The same is also true in many microfluidics systems, especially those operating with liquids. For example, in Newtonian liquid flows at micrometer-length scales it has been well established that under standard conditions the basic continuum laws governing fluid flow, expressed by the equations of mass ~~conservation~~ and momentum, and the no-slip boundary condition at walls, remain valid [25, 51, 58–60]. For water, the continuum assumption is not expected to break down when the channel dimensions are above 1 μm [5]. For molecules such as water, the ratio of molecular size (∼0.3 nm) to geometric length scale (typically on the order of tens to hundreds of microns) is $\sim 10^{-5}$–10^{-6}. As such, it is considered that there are enough molecules at each location within the flow (the concept of fluid particle as a small volume with a large number of molecules is useful) and that the molecules are small enough to treat the flow under the continuum theory [24]. This remains valid even for more complex fluid flows, including high-molecular-weight polymeric solutions, as attested by the agreement between experimental and numerical data in microfluidics, which provides further credibility to this assumption [55, 61, 62].

However, there are a number of exceptions to the validity of the continuum hypothesis as the characteristic length scales of the flow decrease significantly [63, 64], namely when considering gas flows or gas–liquid flows, in which the gas density is very low compared to liquids. In gas flows, the Knudsen number representing the ratio between the mean free path of molecules and the characteristic length scale of the flow is used to evaluate the validity of the continuum approach. Based on the experimental evidence, it is generally accepted that for Knudsen numbers below 0.01 the continuum approximation is valid. For Knudsen numbers above 0.01, there are deviations to the continuum theory, which are handled initially with corrections and subsequently by other theories that describe microscale flow [57, 58, 65].

The other notable exception is related to complex fluids that are composed of large particles in suspension (e.g., red blood cells) or long molecules such as DNA or even polymers of high molecular weight. The radius of gyration of a polymer chain or the characteristic radius of a suspended particle typically varies from 1 nm to 10 μm. As such, for particle/molecule sizes in the high end of the range, assuming a continuum can be misleading since the working fluid may not be well approximated as microstructurally homogeneous [66]. In this case, other methods should be used to properly model the flow.

Although it is important to be aware of cases where the validity of the continuum approximation breaks down, in all situations of relevance to this chapter, the typical dimensions of molecules and channels are within the range of application of the continuum approach.

6.2
Mixing in Microfluidics

6.2.1
Challenges of Micromixing

Efficient mixing may be defined as a procedure for homogenizing an otherwise inhomogeneous system in the shortest possible amount of time and using the least amount of energy [67]. Mixing is required for many practical applications, in particular in association with chemical reaction. Furthermore, rapid mixing is often an essential requirement to achieve a good performance in many microfluidic applications, namely for biochemistry analysis, drug delivery, sequencing and synthesis of nucleic acids, protein folding, and chemical analysis or synthesis.

In macroscale devices, fluid mixing can often be readily achieved by inducing turbulent flow. In contrast, though not impossible, turbulence is more difficult to reach in microfluidic systems due to the reduced length scale of the channels. Additionally, in many microfluidic applications associated with biological systems, the velocity of the flow cannot be too high since high velocities may lead to large shear stresses that can damage cells and compromise their function [15]. Therefore, in the large majority of cases, microfluidic flows take place in the laminar regime, and often at low Reynolds numbers.

The steady laminar flow of Newtonian fluids in ducts is deterministic. When the Reynolds numbers are low, fluids do not mix advectively when different streams come together in a straight microchannel. Instead, the fluid streams flow in parallel as shown in Figure 6.4, with mixing occurring only due to molecular diffusion across the interface between the streams. At this point, it is useful to introduce the dimensionless Péclet number, which expresses the relative importance of the convective over the diffusive mass transport

$$Pe = UL/D \tag{6.5}$$

where D is the diffusion coefficient. For typical microfluidic flow conditions, Pe is generally higher than 10, which means that the diffusion process acts more slowly

Figure 6.4 Junction of two Newtonian fluid streams in a microfluidic device under low *Re* flow conditions.

than the hydrodynamic transport. Additionally, advection is often parallel to the main flow direction and is not useful for the transversal mixing process [19].

Considering a two-dimensional system for simplicity, the mean residence time of a fluid element in the channel, t_R, can be estimated as the ratio between the length of the channel, L, and the average velocity, U,

$$t_R = L/U \tag{6.6}$$

and the time for diffusion (t_D), that is, the time a molecule takes to diffuse a distance d, is given by

$$t_D = d^2/2D \tag{6.7}$$

In general, the smaller the molecule, the larger the diffusion coefficient and the faster the molecule can diffuse. Diffusion coefficients for common liquids are quite low (as compared to gases, for example) and can vary widely. For example, small ions in water have diffusion coefficients around $D = 2 \times 10^{-9}$ $m^2 s^{-1}$, while a large molecule like hemoglobin (in an aqueous solution) has a diffusion coefficient more than two orders of magnitude lower $D = 7 \times 10^{-12}$ $m^2 s^{-1}$. Thus, small ions take around 5 s to diffuse 100 μm in water, while hemoglobin takes almost 25 min to diffuse over the same 100 μm.

Besides the diffusion coefficient, the other crucial parameter to evaluate the mixing time due to diffusion is the relevant length for mixing (cf. Eq. (6.7)). For example, a protein of 70 kDa requires only 1 s to diffuse 10 μm but more than 10 days to diffuse 1 cm [16]. Taken together, these two effects very often imply that mixing times due to diffusion can be very long relative to the residence time of the fluid in the microchannel. Increasing the channel length implies increasing the pressure drop across the channel and therefore the requirements for micropumping and channel structural strength become more demanding [68]. Additionally, in many reactive systems, having such long mixing times/lengths is not admissible and alternative solutions must be sought.

In summary, liquid mixing at the microscale is not a straightforward task [9] as typical length scales of microfluidic devices are too small to experience mixing induced by turbulence and often too large for diffusion to happen fast enough to provide adequate means of mixing [33, 69]. This means that in most cases, alternative strategies must be implemented for micromixing enhancement.

6.2.2 Overview of Methods for Micromixing Enhancement

Since mixing by molecular diffusion is generally not efficient, other mechanisms need to be brought into action, such as secondary flows due to fluid nonlinearities, flow instabilities, or external actuators. These may be categorized into passive and active methods. Active mixers use external sources to increase the interfacial area between fluid streams, while passive mixers rely on fixed geometrical features (i.e., there are no moving parts) [33], utilize no external energy input, and depend largely

on the mechanism used for generating fluid flow through the microchannel [24]. A good introduction to the general theme of mixing is presented by Ottino [70], and by Nguyen [15] for the particular case of micromixing, and is only briefly summarized below.

One possible approach to enhance mixing, inspired by macromixers, is to use active methods to perturb the low Reynolds number flows. Active mixing requires external forcing to induce a flow disturbance and hence increases the amount of transverse flow within the channel. These forces may come from moving mechanical parts and/or external actuators [71]. Active mixers usually produce high levels of mixing, but the systems are considerably more complex, may be difficult to integrate into microfluidic devices, and can be expensive to manufacture [24]. A particular challenge is related to the dominance of surface effects over volume effects as the systems are miniaturized. As a consequence, actuation concepts based on volume forces (e.g., magnetic stirrer), which are widely used at the macroscale, become less efficient at the microscale [15].

The actuator for active mixing can be a pump or works as an energy source, for example, pulsating side flow [72], micropumping for stopping and restarting the flow [73], application of unsteady electric fields acting on the fluid or on suspended particles [74], application of potential differences across pairs of electrodes within the microchannel in the presence of an external magnetic field [75, 76], application of thermal gradients to induce disturbances in the flow using either thermopneumatic actuators (based on the thermal expansion of gases), thermal-expansion actuators (based on the thermal expansion of solids) and bimetallic actuators (based on the difference in thermal coefficient of expansion of two bonded solids) [15], or application of acoustic fields [77, 78]. For further details, the reader is referred to [15, 79]. Active principles can also obviously be used in combination with passive techniques.

Another alternative to reduce mixing times is to induce stirring by chaotic advection [80], with final mixing by diffusion, a process that has also been used in microfluidics [81, 82] and requires a non-negligible Reynolds number since chaotic advection is inherently a nonlinear inertial effect. This is usually accomplished in various ways, depending on the flow Reynolds number, but invariably the flow becomes time-dependent and can also be three-dimensional [19]. If the Reynolds number is low and the fluid is Newtonian, the use of 2D obstacles is usually insufficient to create chaotic advection and enhance mixing. Asymmetric and 3D arrangements of flow perturbations, such as grooves, obstacles, and duct twists become necessary to impart the stretching, reorientation, and randomization mechanisms of distributive mixing [19, 83]. Micromixing in Newtonian fluids by chaotic advection is reviewed in detail by Nguyen [15].

Fluids in microsystems very often contain additives that impart non-Newtonian characteristics to the fluids and, in particular, viscoelasticity. These rheological characteristics introduce nonlinearities that can be explored to dramatically change the flow dynamics, and in particular to enhance mixing [1, 54, 84]. The elasticity of the fluids is characterized, among other things, by the appearance of anisotropic normal stresses, which produce secondary flows [85] and/or elastic instabilities even

at extremely low Reynolds number. Although weak, these secondary flows help the appearance of flow instabilities and reduce mixing times, because they create conditions similar to those of chaotic advection, that is, 3D flow which we call here chaotic elastic flow (inertia is negligible). The elastic instabilities have been shown to exist even in the absence of inertia and are associated with strong curvature of streamlines and large normal stresses [86]. When the elastic instabilities become very intense, reaching a saturated nonlinear state, fluctuations even become random over a wide range of length and time scales [87], very much like inertial turbulence, in spite of negligible Reynolds numbers. This has prompted Groisman and Steinberg [88] to call it "elastic turbulence." So, elastic effects are used to reduce the critical conditions for the existence of chaotic flow and enhanced mixing, allowing the use, at lower Reynolds numbers, of passive techniques usually associated with higher Reynolds number flows. This type of passive mixing is discussed in detail in Section 6.5. Before that, however, we introduce in Section 6.3 some basic concepts about non-Newtonian fluids, as well as the governing equations required for flows of complex fluids (Section 6.4).

6.3 Non-Newtonian Viscoelastic Fluids

In this section, we present a brief overview of the rheology of non-Newtonian fluids. More detailed descriptions are found in [45, 46], among others. Rheometry is also described in [89, 90].

The rheology of fluids is assessed through their behavior in a small set of controllable (and quasi-controllable) flows, whose kinematics are known and independent of fluid properties. For shear-based properties, this is the Couette flow schematically shown in Figure 6.5 in the planar (2D) version. Technologically, the Couette flow is usually implemented in an axisymmetric version, as in the concentric cylinders, cone–plate, or plate–plate geometries for which the applied torque and rotational speed are directly proportional to the shear stress and shear rate, respectively. The use of small gaps in these geometries ensures a controllable flow and a nearly constant shear rate across the gap. For extensional-based properties the ideal flow is a purely extensional flow, such as the uniaxial extension, but it is not always possible to implement it easily, especially for low-viscosity fluids.

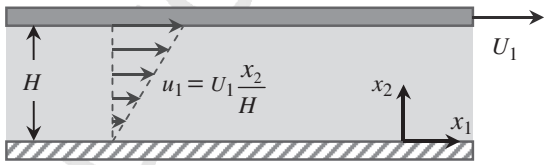

Figure 6.5 Plane Couette flow and coordinate system.

6.3.1
Shear Viscosity

Shear viscosity is defined as the ratio between shear stress (τ_{12}) and the shear rate ($\dot{\gamma}$) in the Couette flow of Figure 6.5, where subscripts 1 and 2 denote streamwise and transverse directions, respectively:

$$\eta = \frac{\tau_{12}}{du_1/dx_2} = \frac{\tau_{12}}{U_1/H} = \frac{\tau_{12}}{\dot{\gamma}} \tag{6.8}$$

Typically, non-Newtonian fluids have a shear-thinning behavior with a low shear rate constant viscosity plateau, as shown in Figure 6.6. A second lower constant viscosity plateau at high shear rates is also frequent, but often this is not observed in rheometric flows before the onset of flow instabilities. Some suspensions of irregular solids, or surfactant solutions, exhibit a shear-thickening behavior, but this is often limited to a narrow range of shear rates.

There are materials for which the first Newtonian plateau of the shear viscosity is not observed, and the shear viscosity grows to infinity at vanishingly small shear rates. These materials possess some form of internal structure for which a minimum stress is required prior to yielding – the yield stress – and often their viscosity depends not only on the shear rate but also on time – thixotropy or anti-thixotropy, depending on whether the shear viscosity increases or decreases over time. Examples are tooth-paste, mayonnaise, blood, and suspensions of particles, in which the effect is enhanced if macromolecules are present. Dilute and semidilute polymer solutions do not exhibit yield stress and thixotropy, so these properties will not be considered

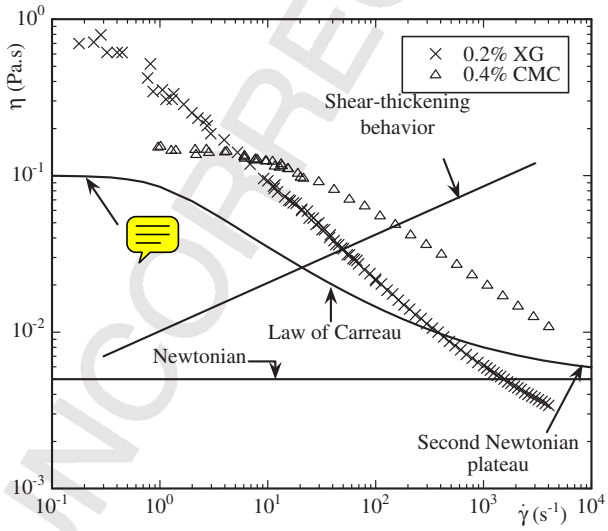

Figure 6.6 Shear viscosity of aqueous solutions of 0.2% by weight xanthan gum (XG) and 0.4% by weight carboxy methyl cellulose (CMC) and typical behavior of some rheological models.

further. The interested reader is referred to Larson [46] and additional papers on issues and techniques involving yield stress fluids [91–95].

6.3.2 Normal Stresses

Viscoelastic fluids develop normal stresses in shear flow, which are known within a constant value, so their differences are the useful material properties. For a pure shear flow as illustrated in Figure 6.5, the first normal stress difference (N_1) is defined as the difference between the streamwise normal stress (τ_{11}) and the transverse normal stress (τ_{22}), and gives rise to the material property designated as first normal stress difference coefficient, Ψ_1:

$$\Psi_1 \equiv \frac{N_1}{\dot{\gamma}^2} = \frac{\tau_{11}-\tau_{22}}{\dot{\gamma}^2} \tag{6.9}$$

The second normal stress difference is $N_2 \equiv \tau_{22}-\tau_{33}$ and the corresponding coefficient is $\Psi_2 = N_2/\dot{\gamma}^2$. N_2 is usually small, with maximum values not exceeding 20% of N_1 and with an opposite sign to N_1. Measurement of N_2 is difficult and can be done using a special cone–plate apparatus [96].

The typical behavior of a viscoelastic fluid regarding Ψ_1 is included in Figure 6.7, which pertains to an aqueous solution of polyacrylamide (PAA) at a weight concentration of 300 ppm [97]. In the limit of small shear rates, Ψ_1 tends to a constant value, to which corresponds $N_1 \to 0$. So, even though the behavior of Ψ_1 depicted in Figure 6.7 is shear-thinning, the normal stresses grow quickly as N_1 varies with the square of the shear rate (when Ψ_1 is constant). N_1 is responsible for some spectacular phenomena, such as the Weissenberg effect [45]. Today, the capability of measurement of N_1 is standard in commercial rotational rheometers.

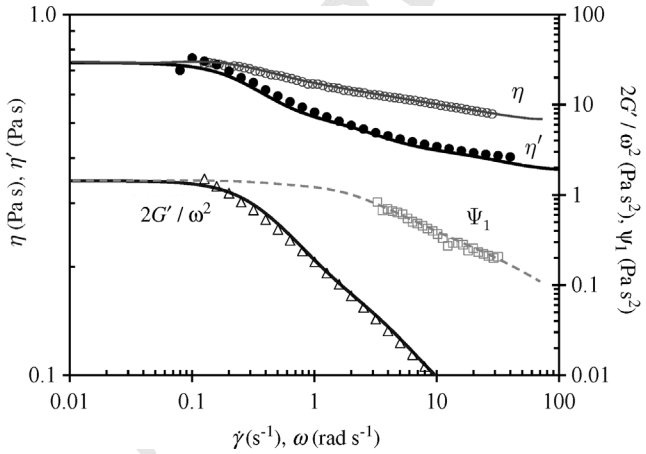

Figure 6.7 Material functions of a 300-ppm PAA solution under steady shear and SAOS flows. Details of fluid composition can be found in [97].

6.3.3
Storage and Loss Moduli

In small amplitude oscillatory shear (SAOS) flow of a viscoelastic fluid, an oscillating shear stress, $\tau = \tau_0 \sin(\omega t)$, is applied to one of the walls of the Couette cell (alternatively, an oscillatory deformation can be applied, $\gamma = \gamma_0 \sin(\omega t)$, and the corresponding shear stress measured). The ensuing fluid deformation will be given by $\gamma(t) = \gamma_0 \sin(\omega t + \delta)$, and is out of phase by δ relative to the applied stress. Provided the amplitude of deformation is small, the response of the material depends only on the forcing frequency and the resulting storage (G') and loss (G'') moduli are mathematically defined as

$$G' = \omega \eta'' \equiv \frac{\tau_0}{\gamma_0} \cos\delta; \qquad G'' = \omega \eta' \equiv \frac{\tau_0}{\gamma_0} \sin\delta \tag{6.10}$$

which measure the amount of energy stored reversibly by the material (G', deformation in phase with the stress) and consequently can be recovered, and the energy irreversibly lost by viscous dissipation (G'', deformation out of phase with the stress). Sometimes the components η' and η'' of the complex dynamic viscosity (η^*) are used instead, where $\eta^* = \eta' - i\,\eta''$, with i representing the imaginary number ($i^2 = -1$).

For a Newtonian fluid, the response in this test would be obvious ($G' = 0$, $G'' = \tau_0/\gamma_0$) so the loss angle (δ) would be maximum and given by $\delta = \pi/2$ (note that $\tan\delta = G''/G'$).

6.3.4
Extensional Viscosity

In a pure extensional flow, the velocity vector only varies in its direction, as in a traction or compression experiment. If a fluid sample is subject to an extensional flow, such as the flow in a contraction or in a pulling device (cf. Figure 6.8), it undergoes an extensional deformation and develops normal stresses proportional to the normal strain rate ($\dot{\varepsilon}$). The ratio between the normal stress difference and the strain rate defines the extensional viscosity

$$\eta_E \equiv \frac{\tau_{11} - \tau_{22}}{\partial u_1/\partial x_1} = \frac{\tau_{11} - \tau_{22}}{\dot{\varepsilon}} \tag{6.11}$$

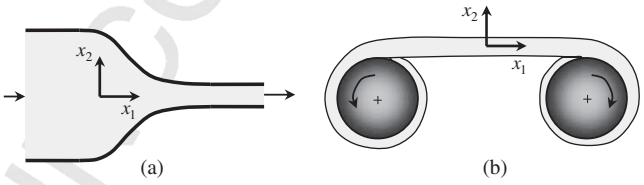

Figure 6.8 Schematic representation of a flow with a strong extensional deformation: (a) smooth contraction flow; (b) extensional flow device.

Note that all fluids, including Newtonian fluids, have a nonzero extensional viscosity. For Newtonian fluids, the uniaxial extensional viscosity equals three times the shear-viscosity, so no distinction is required, but for viscoelastic fluids the ratio between the extensional and shear viscosities, called the Trouton ratio, varies with the rate of deformation and can largely exceed the value of three, attaining sometimes values of the order of 100 or higher. An impressive consequence of a very high extensional viscosity is the tubeless siphon experiment [45].

The measurement of the extensional viscosity is not easy, because it is difficult to ensure that fluid particles are under a constant strain rate for a sufficiently long time to eliminate transient start-up effects, especially at high strain rates. Additionally, for the mobile systems of interest here it is difficult to impose a constant strain rate flow and so the extensional viscosity can only be directly measured with such devices as the capillary break up extensional rheometer (CaBER) [98]. A variant of the CaBER is the filament stretching extensional rheometer (FiSER) based on the work of Tirtaatmadja and Sridhar [99], where the fluid filament between plates is deformed as the plates move with a velocity increasing exponentially with time. This allows the measurement of strain-dependent extensional viscosity [100].

Alternatively, there are flows with a strong extensional nature from which an extensional viscosity indexer can be obtained, such as the pressure drop enhancement in a contraction flow or the tensile force required to sustain fluid stretching in the space between two nozzles in the opposed jet rheometer, but in these flows the fluids are not subject to a constant strain rate and the flow is contaminated by secondary effects that may overwhelm the main measurement. In contrast, the high consistency of polymer melts facilitates the integrity of fluid samples under uniaxial extension and a number of devices can be used to measure their extensional viscosity, such as the Sentmanat device [101].

6.3.5
Other Rheological Properties

The rheological properties discussed can today be reliably measured and are standard. However, it is clear to rheologists and fluid dynamicists alike that the set does not guarantee that if a rheological constitutive equation is able to predict all of them for a particular fluid, it will be able to predict accurately all types of flow with that fluid [102, 103], a situation quite similar to the prediction of Newtonian turbulent flows. This indicates the need for other fluid properties, especially those related to time-dependency and nonlinear effects.

Other tests, such as the creep and the stress relaxation flows in shear and strain, are good examples. One may also consider the response of fluids to a sequence of steps in normal or shear strain, since here the response of fluids is different from that to a single step. To assess nonlinear viscoelasticity, meaningful interpretation of data from large amplitude oscillatory shear flow (LAOS) is currently under development [104].

6.4 Governing Equations

Viscoelastic fluid flow is governed by the momentum and continuity equations together with a rheological constitutive equation adequate for the fluid. If heat transfer is involved, the energy equation must be included with the corresponding thermal constitutive equation, usually Fourier's heat law. To consider chemical reaction, the mass conservation equation for each chemical species needs to be solved in combination with the mass transport constitutive equation, usually Fick's law. To assess mixing performance, it may be necessary to solve a transport equation for an adequate scalar. These equations are coupled in a variety of ways: dependence of fluid properties on temperature, molecular orientation and/or fluid composition, through new terms in the governing equation, such as buoyancy in the momentum equation or extra terms in the constitutive equation, which can be traced back to the effect of temperature on the mechanisms acting at microscopic level. The treatment of these extra terms of the constitutive equations is an advanced topic not considered here. For a more in-depth discussions, the reader is referred to [105–107].

In general, the fluid dynamics and heat transfer problems are coupled and the set of governing equations has to be solved simultaneously. For a general flow problem, this can only be done numerically, but under simplified conditions, such as temperature-independent fluid properties (a good approximation, if temperature variations are small), it is possible to solve for the flow without consideration for the thermal problem (although not the other way around). Other times, the solution can still be obtained assuming temperature-independent properties, but a correction is introduced to compensate for the neglected effect. This is a fairly successful approach for simple geometries and simple fluids (such as inelastic fluids), but for viscoelastic fluids a more exact approach may be required for accurate results [108].

The governing equations are presented in the next sections in tensor notation for generality. The reader is referred to the appendices of Bird *et al.* [45, 109, 110] for an extensive presentation of their form in various coordinate systems.

6.4.1 Continuity and Momentum Equations

The continuity equation is written as

$$\frac{\partial \varrho}{\partial t} + \nabla \cdot (\varrho \mathbf{u}) = 0 \tag{6.12}$$

and the momentum equation as

$$\frac{\partial (\varrho \mathbf{u})}{\partial t} + \varrho (\mathbf{u} \cdot \nabla)\mathbf{u} = -\nabla p + \varrho \mathbf{g} + \nabla \cdot \tau_t + \varrho_e \mathbf{E} - \frac{1}{2}\mathbf{E} \cdot \mathbf{E} \in_0 \nabla \in + \frac{\in_0}{2} \nabla \left(\varrho \frac{\partial \in}{\partial \varrho} \mathbf{E} \cdot \mathbf{E} \right) \tag{6.13}$$

where $\mathbf{u}$ is the velocity vector, p is the pressure, ϱ is the fluid density, and the fluid total extra stress (τ_t) is given by an adequate rheological constitutive equation. The last

three terms on the right-hand side take electrokinetic effects into account, where ϱ_e denotes the net electric charge distribution within the fluid, $\mathbf{E}$ represents the applied electric field (or induced streaming potential in flows with electroviscous effects), $\in_0$ is the dielectric permittivity of vacuum, and $\in$ is the dielectric constant of the fluid. The last term accounts for permittivity variations with fluid density and is only relevant at gas–liquid interfaces or in ionized gas flows, whereas the penultimate term accounts for spatial variations in the dielectric constant of the fluid. Thus, for incompressible fluids of constant dielectric permittivity only the first of the three terms is required, which is known as Lorentz force.

The applied electric field intensity can be related to the imposed electric potential $\mathbf{E} = -\nabla\phi$ and similarly the induced charge is related to the induced potential ψ. In this chapter, we will assume that they are independent of each other and therefore they can be linearly combined into the total electric potential $\Phi = \phi + \psi$. This is admissible when the EDL is thin, and also requires a weak applied streamwise gradient of electrical potential, that is, $\Delta\phi/L \ll \psi_0/\zeta$, where $\Delta\phi$ is the potential difference of the applied electrical field, L is the distance between the electrodes, and ζ is the Debye layer thickness. In this case, the transverse charge distribution is essentially determined by the potential at the wall, ψ_0, the so-called zeta potential. If the local EOF velocities are small and/or parallel to the walls, as in thin EDLs, the effect of fluid motion on the charge distribution can also be neglected. These simplifications are part of the so-called standard electrokinetic model, in which case Eq. (6.13) becomes

$$\frac{\partial(\varrho\mathbf{u})}{\partial t} + \varrho(\mathbf{u}\cdot\nabla)\mathbf{u} = -\nabla p + \varrho\mathbf{g} + \nabla\cdot\tau_t - \varrho_e\nabla\Phi \tag{6.14}$$

6.4.2 Rheological Constitutive Equation

The fluid total extra stress (τ_t) is given as the sum of an incompressible solvent contribution having a viscosity coefficient η_s and a polymer/additive stress contribution τ_p, as

$$\tau_t = 2\eta_s(II_{\mathbf{D}}, III_{\mathbf{D}})\mathbf{D} + \tau_p \tag{6.15}$$

The solvent viscosity coefficient in Eq. (6.15) has been made to depend on the second and third invariants ($II_{\mathbf{D}}$, $III_{\mathbf{D}}$) of the rate of deformation tensor $\mathbf{D}$ defined as

$$\mathbf{D} = \frac{1}{2}\left(\nabla\mathbf{u} + \nabla\mathbf{u}^{\mathrm{T}}\right) \tag{6.16}$$

to consider both the possibility of having a Newtonian (constant viscosity) or a non-Newtonian (variable viscosity) solvent. In this way, Eq. (6.15) includes the class of inelastic non-Newtonian fluids known as generalized Newtonian fluids (GNF) for which the polymer contribution is set to zero ($\tau_p = \mathbf{0}$). Then, the viscosity coefficient depends on invariants of the rate of deformation tensor, the most common being the second invariant, defined in the next section. For viscoelastic fluids, η_s is set to zero

for polymer melts or to a nonzero constant when dealing with a polymer solution based on a Newtonian solvent.

Usually the non-Newtonian fluids are treated as incompressible fluids, so the continuity equation simplifies to $\nabla \cdot \mathbf{u} = 0$. Some very limited phenomena may require consideration of liquid compressibility, an issue not considered here.

6.4.2.1 Generalized Newtonian Fluid Model

The purely viscous GNF model is defined in Eq. (6.15) with $\tau_p = \mathbf{0}$ and the fluid viscosity $\eta_s(II_\mathbf{D}, III_\mathbf{D})$ depending on invariants of the rate of deformation tensor [111]. The most common models consider only dependence on the second invariant and we can write many of them in a compact form as

$$\eta_s(II_\mathbf{D}) = (\eta_1 - \eta_2)[\alpha + (\Lambda II_\mathbf{D})^a]^{\frac{n-1}{a}} + \eta_2 \quad \text{with} \quad II_\mathbf{D} \equiv \sqrt{2\mathbf{D} : \mathbf{D}} \tag{6.17}$$

Equation 6.17 includes the Newtonian fluid model (viscosity coefficient η), the Ostwald de Waele power law (consistency index K and power index n), the Carreau–Yasuda model (zero shear viscosity η_0, infinite shear rate viscosity η_∞, power index n, transition coefficient a, and transition time scale Λ), the simplified Carreau model and the Sisko model, with the corresponding coefficients given in Table 6.1.

6.4.2.2 Viscoelastic Stress Models

The previous constitutive models cannot predict viscoelastic characteristics, such as any shear-induced normal stresses in Couette flow, or memory effects. There is a class of models, which is still explicit on the stress tensor that can predict some of these elastic effects. One such model, the Criminale– Eriksen– Filbey (CEF) equation, should only be used in steady shear flow in which case it provides accurate results [45]. The CEF model can be written as

$$\tau = 2\eta(\dot{\gamma})\mathbf{D} - \Psi_1(\dot{\gamma})\overset{\nabla}{\mathbf{D}} + 4\Psi_2(\dot{\gamma})\mathbf{D}^2 \tag{6.18}$$

with $\dot{\gamma} \equiv II_\mathbf{D}$ and $\overset{\nabla}{\mathbf{D}}$ representing the upper-convected derivative of $\mathbf{D}$, defined as

$$\overset{\nabla}{\mathbf{D}} \equiv \frac{\partial \mathbf{D}}{\partial t} + (\mathbf{u} \cdot \nabla)\mathbf{D} - \nabla\mathbf{u}^\mathrm{T} \cdot \mathbf{D} - \mathbf{D} \cdot \nabla\mathbf{u} \tag{6.19}$$

Table 6.1 Values of parameters in generalized viscosity function of Eq. (6.17) for some typical viscosity models.

	N	a	α	η_1	η_2	Λ	*
Newtonian	1	Any	Any	η	0	Any	
Power law	n	Any	0	*	0	*	$K = \eta_1 \Lambda^{n-1}$
Carreau–Yasuda	n	Any	1	η_0	η_∞	Λ	
Simplified Carreau	n	2	1	η_0	0	Λ	
Sisko	n	Any	0	*	η_∞	*	$K = (\eta_1 - \eta_2)\Lambda^{n-1}$

Other stress explicit models for viscoelastic fluids are contained in Eq. (6.18), such as the second-order fluid (constant η, Ψ_1, and Ψ_2) or the Reiner–Rivlin equation ($\Psi_2 = 0$). The use of these models should be restricted to weakly elastic fluids and low Weissenberg number flows, that is, to fluids deviating slightly from Newtonian and to slow flows, since outside these conditions they lead to physically incorrect predictions. So, these models are essentially useful to investigate deviations from the behavior of Stokes ~~fluids~~.

More useful are the integro-differential viscoelastic fluid models. The polymeric contribution to the extra-stress tensor in Eq. (6.15) can in general be represented as a set of N modes

$$\tau_p = \sum_{k=1}^{N} \tau_k \tag{6.20}$$

where each polymer mode obeys a rheological equation of state of integral or differential nature. An example of the latter is the following general equation:

$$f(\mathrm{tr}\,\tau)\tau + \frac{\lambda}{F(\mathrm{tr}\,\tau, L^2)}\overset{\square}{\tau} + \frac{\alpha\lambda}{\eta_p}\tau^2 = 2\eta_p \mathbf{D} \tag{6.21}$$

which includes such models as the upper-convected Maxwell (UCM) model, the Phan-Thien–Tanner model (PTT), the Johnson–Segalman (JS) model, the Giesekus model or the FENE-MCR model, according to Table 6.2. For conciseness and since very often a single mode is used, the subscript indicating the mode has been dropped. Note that for each mode the model parameters can have different numerical values.

Function $f(\mathrm{tr}\,\tau)$ takes either the exponential form, $f(\mathrm{tr}\,\tau) = \exp[(\varepsilon\lambda/\eta_p)\mathrm{tr}\,\tau]$, or a simpler linearized form $f(\mathrm{tr}\,\tau) = 1 + \left(\varepsilon\lambda/\eta_p\right)\mathrm{tr}\,\tau$, and $F(\mathrm{tr}\,\tau, L^2) = (1 - \mathrm{tr}\,\tau/L^2)^{-1}$. The temperature influences exponentially the polymer viscosity coefficient, η_p, and the relaxation time, $\lambda = \lambda(T_0)a_T$ where T_0 is a reference temperature, and a_T is the nondimensional shift factor, usually described using the Williams–Landel–Ferry (WLF) equation [112]. The shear modulus, $G = \eta_p/\lambda$, is only weakly dependent on the temperature, as discussed by Wapperom *et al.* [113]. The same correction for temperature is valid for the material functions in the constitutive equation (6.17)

Table 6.2 Model parameters of Eq. (6.21) for some viscoelastic constitutive equations.

Models	ε	α	L^2	ξ	β
UCM	0	0	∞	0	0
Oldroyd-B	0	0	∞	0	]0, 1[
PTT[a)]	>0	0	∞	[0, 2]	0[b)]
FENE-MCR	0	0	>0	0	]0, 1[
Giesekus	0	]0, 1[	∞	0	0[b)]

a) If $\xi = 0$ it is also called the simplified PTT (sPTT) model. The original PTT relies on the exponential form of $f(\mathrm{tr}\tau_p)$, a linearized form uses the linear version of $f(\mathrm{tr}\tau_p)$.

b) Strictly speaking $\beta = 0$ for the PTT or Giesekus models. Today their use is widespread to model polymer solutions with a solvent contribution ($\beta \neq 0$) and the designation stands.

and (6.18). $F(\mathrm{tr}\,\tau, L^2)$ is the stretch function that depends on the trace of the stress tensor and on the extensibility parameter L^2, representing the ratio of the maximum to the equilibrium average dumbbell extensions for a FENE-MCR model (from finitely extensible nonlinear elastic, with the Chilcott–Rallison approximation) [114]. The stress coefficient function $f(\mathrm{tr}\,\tau)$ introduces the dimensionless parameter ε, which is closely related to the steady-state elongational viscosity in extensional flow ($\eta_E \propto 1/\varepsilon$ for low ε), while α is the dimensionless mobility factor of the Giesekus equation. Finally, $\overset{\square}{\tau}_p$ denotes the Gordon–Schowalter derivative of the extra-stress tensor, which is a mixture of the upper ($\xi = 0$) and lower ($\xi = 2$) convected derivatives, and is defined as

$$\overset{\square}{\tau} = \frac{\mathrm{D}\tau}{\mathrm{D}t} - \tau \cdot \nabla \mathbf{u} - \nabla \mathbf{u}^{\mathrm{T}} \cdot \tau + \xi\left(\mathbf{D} \cdot \tau + \tau \cdot \mathbf{D}^{\mathrm{T}}\right) \tag{6.22}$$

Parameter ξ accounts for the slip between the molecular network and the continuum medium and provides nonzero second normal stress differences in pure shear flow. However, the use of $\xi \neq 0$ can lead to unphysical behavior of the model, which are called Hadamard instabilities, if the solvent contribution is weak or nonexistent. β in Table 6.2 denotes the solvent ratio, defined as $\beta = \eta_s/(\eta_s + \eta_p)$.

The UCM model is the simplest viscoelastic differential model and is characterized by a constant shear viscosity, equal to η_p, a constant first normal stress difference coefficient ($\Psi_1 = 2\eta_p\lambda$), and a zero second normal stress difference ($N_2 = 0$). Note that the UCM model requires the solvent viscosity in Eq. (6.15) to be set to zero ($\beta, \eta_s = 0$). If the solvent viscosity is a nonzero constant ($\eta_s \neq 0$), we have the so-called Oldroyd-B model, which has the same elastic properties as the UCM model, whereas for the viscous properties it suffices to add the contribution from the Newtonian solvent. The normal stresses/extensional viscosities of the UCM and Oldroyd-B fluid become unbounded in extensional flow when the rate of deformation tends to $1/(2\lambda)$ as is clear from the steady-state uniaxial extensional viscosity given by

$$\eta_E = 3\eta_p \frac{1}{(1+\lambda\dot{\varepsilon})(1-2\lambda\dot{\varepsilon})} + 3\eta_s \tag{6.23}$$

Nevertheless, these two models contain many of the essential features of viscoelasticity and for this reason they are still extensively used, especially in the development of numerical methods or in preliminary calculations with viscoelastic fluids (a robust method for the UCM and Oldroyd-B models is likely to be robust for other constitutive equations). Additionally, the Oldroyd-B model is adequate to describe the behavior of Boger fluids (constant viscosity elastic fluids). These are mostly dilute polymer solutions in high-viscosity Newtonian solvents, but it is also possible to manufacture them with solvents of moderate viscosity provided these are poor solvents [115].

Regarding the response to SAOS flow, the described viscoelastic models behave identically with their loss and storage moduli given by

$$G' = \eta''\omega = \frac{\eta_p\lambda\omega^2}{1+(\lambda\omega)^2}; \qquad G'' = \eta'\omega = \eta_s\omega + \frac{\eta_p\omega}{1+(\lambda\omega)^2} \tag{6.24}$$

Figure 6.7 shows G' and G'' (via η') as a function of the frequency of oscillation for a 300-ppm aqueous solution of PAA and the corresponding fit by a three-mode polymer model with a Newtonian solvent contribution.

The prediction of variable viscosity and normal stress difference coefficients is provided by the more complex models, such as the PTT, Giesekus, or others. The nonlinear fluid properties are precisely introduced by the nonlinear terms of the equations, with different parameters having different impacts onto the model. Usually, the addition of shear-thinning to the shear viscosity also leads to shear-thinning of Ψ_1 and for $\Psi_2 \neq 0$ it is necessary for the coefficient ξ inside the Gordon–Schowalter derivative to be nonzero, or instead to have the quadratic stress term switched on, as in the Giesekus model.

There are more models for polymer solutions and lately they have been derived on the basis of molecular kinetic theories for polymer molecules, such as the FENE-P model (finitely extensible nonlinear elastic with Peterlin's approximation). For polymer melts, there is also a large set of complex network-based models. All modern constitutive equations have an involving formulation, frequently introducing the concepts of conformation tensor, or of stretch and orientation tensors, among others. As an example, we give below the constitutive equation for the FENE-P model written in terms of the conformation tensor $\mathbf{A}$, which up to a scaling factor corresponds to the second moment of the distribution function of the end-to-end vector of the model dumbbell, $< \mathbf{QQ} >$, via [107]:

$$\tau_p = \frac{\eta_p}{\lambda}[f(\mathrm{tr}\,\mathbf{A})\mathbf{A} - \mathbf{I}] \tag{6.25}$$

with

$$f(\mathrm{tr}\,\mathbf{A})\mathbf{A} + \lambda \overset{\nabla}{\mathbf{A}} = \mathbf{I} \quad \text{and} \quad f(\mathrm{tr}\,\mathbf{A}) = \frac{L^2}{L^2 - \mathrm{tr}\,\mathbf{A}} \tag{6.26}$$

where L^2 represents the maximum extensibility of the dumbbell.

For more details and models, see the works of Larson [116], Bird *et al.* [45, 109], and more recently Huilgol and Phan-Thien [117], Larson [46], and Tanner [103].

6.4.3 Equations for Electro-Osmosis

To solve Eq. (6.14) for electrically driven flows, it is necessary to determine the electric charge distribution density. Figure 6.9 illustrates the principle of EO in a simple channel. Basically, when a polar fluid is brought in contact with a surface chemical equilibrium leads to a spontaneous charge being acquired by the wall and simultaneously by the layers of fluid nearer to the surface (with ions of opposite sign, the counter-ions), thus forcing the formation of a near-wall layer of immobile ions followed by a second layer of mobile ions, both of which contain a higher concentration of counter-ions as the co-ions are repelled by the wall [118]. The layer of immobile ions, the Stern layer, and the immediate layer with mobile ions, the diffuse layer, form together the so-called EDL. EOF is obtained when an external field

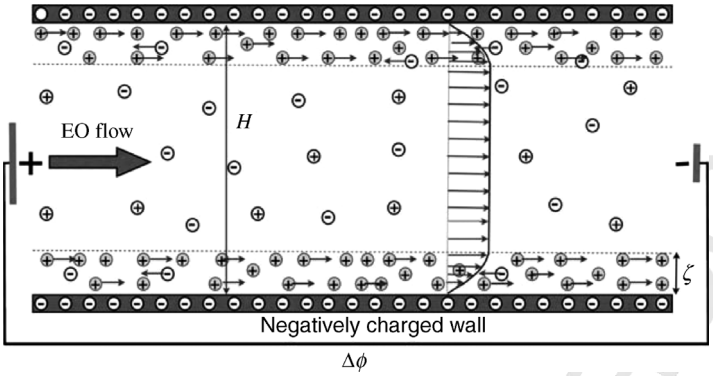

Figure 6.9 Illustration of EO driven flow. The blue and red arrows are Coulombic repulsive and attractive forces on the counter and co-ions, respectively. Adapted from [118].

$\mathbf{E} = -\nabla\phi$ (ϕ is the potential in the streamwise direction) is applied between the channel inlet and outlet thus creating Coulomb forces acting on the charges within the EDL. The motion of these ions drags the remaining fluid laying outside the EDL along the channel. To determine the Coulomb force (last term on the right-hand side of Eq. (6.14)), it is necessary to quantify the net electric charge density, ϱ_e, which is given by

$$\varrho_e = e\sum_i z_i n_i \tag{6.27}$$

where e is the elementary charge, n_i is the bulk number concentration of positive/negative ion i, and z_i is the corresponding ion valence. Note that the bulk number ionic concentration n is related to the molar concentration of ions (c_i) in the electrolyte solution via $n_i = N_A c_i$, where N_A is Avogadro's number [4]. The simplest case is that of electrolytes with equally charged ions of valence $z^- - z^+$ for which the above general Eq. (6.27) simplifies to $\varrho_e = e\,z(n^+ - n^-)$.

The spontaneously induced potential ψ near the interface/wall is given by

$$\nabla^2\psi = -\frac{\varrho_e}{\in} \tag{6.28}$$

whereas the imposed streamwise potential is such that

$$\nabla^2\phi = 0 \tag{6.29}$$

To determine the ionic concentration, their transport equations, also called the Nernst–Planck equations, need to be solved. These are expressed as

$$\frac{\partial(n^\pm)}{\partial t} + \mathbf{u}\cdot\nabla n^\pm = \nabla\cdot\left(D^\pm\nabla n^\pm\right) \pm \nabla\cdot\left[D^\pm n^\pm \frac{ez}{k_B T}\nabla(\phi+\psi)\right] \tag{6.30}$$

where $D^\pm$ are the diffusion coefficients of the $n^\pm$ ions, respectively, k_B is Boltzmann's constant, and T is the absolute temperature. Simpler models can be used in simpler

situations: when flow is essentially unidirectional, steady, and parallel to walls, the ionic distribution becomes stationary and the EDL is restricted to the wall vicinity, so significant variations of $n^{\pm}$ and ψ only occur in the direction normal to the wall and in its vicinity. Then, the Nernst–Planck equations reduce to the stable Boltzmann distribution and the corresponding electric charge density is given by

$$\varrho_e = -2\, n\, e\, z\, sinh\left(\frac{ez}{k_B T}\psi\right) \tag{6.31}$$

Equations (6.28) and (6.31) constitute the so-called Poisson–Boltzmann model, which is still quite general. When the ratio between the electric to thermal energies is small, synonymous of a small value of $e\,z\,\psi_0/(k_B T)$ (ψ_0 is the zeta potential), the hyperbolic sine function can be linearized ($\sinh x \approx x$) and the electric charge density becomes

$$\varrho_e = - \in \kappa^2 \psi \tag{6.32}$$

where $\kappa^2 = 2e^2 z^2 n/(\in k_B T)$ is the Debye–Hückel parameter related to the thickness of the EDL, $\zeta = 1/\kappa$. Equations (6.28) and (6.32) constitute the Poisson–Boltzmann–Debye–Hückel model.

6.4.4 Thermal Energy Equation

For nonisothermal flows, it is necessary to include in the set of governing equations the following special form of the energy equation:

$$\varrho c \frac{\mathrm{D}T}{\mathrm{D}t} = -\nabla \cdot \mathbf{q} + \dot{q}_1 + \tau_t : \mathbf{D} \tag{6.33}$$

where c is the specific heat of the fluid, $\mathbf{q}$ is the conduction heat flux to be quantified below, and $\dot{q}_1$ is a source, here representing Joule heating per unit volume. The last term on the right-hand side represents the mechanical energy supply by the viscoelastic medium (the viscoelastic stress work), which includes the viscous dissipation. This is an important term since many non-Newtonian viscoelastic fluids are highly viscous and have non-negligible internal viscous dissipation, which precludes an isothermal approach. The small channel dimensions in microfluidics, if coupled with large fluid velocities, lead to large shear rates, and the viscoelastic stress work becomes non-negligible.

In rigorous terms, the last term of Eq. (6.33) should have been multiplied by a coefficient κ and an extra term multiplied by $(1-\kappa)$ should have been added to the energy equation in order to account for internal energy storage by the viscoelastic medium [107]. The connection between viscoelasticity and thermal energy and the more specific issue of the numerical value of κ are still topics of research [119] and numerical simulations of Peters and Baaijens [120] have also shown that the results from such an extended equation for viscoelastic fluids are not too different from those obtained with the simpler Eq. (6.33), which neglects the extra internal energy storage term (for pure shear flow, the results are actually exactly the same).

For the diffusive heat flux, Fourier's law of heat conduction is assumed with an isotropic thermal conductivity k

$$\mathbf{q} = -k\nabla T \tag{6.34}$$

For materials possessing some form of orientational order, such as liquid crystals, the thermal conductivity can have an anisotropic behavior and is now a second-order tensor ($\mathbf{k}$), in which case the heat flux is given by $\mathbf{q} = -\mathbf{k}\cdot\nabla T$.

The Joule heating effect is a consequence of the application of an electric field across a conductive fluid (as in EO) and is given in complete form by

$$\dot{q}_1 = \frac{1}{\sigma}(\varrho_e\mathbf{u} + \sigma\mathbf{E})\cdot(\varrho_e\mathbf{u} + \sigma\mathbf{E}) \tag{6.35}$$

where σ represents the electrical conductivity of the fluid. Under the conditions of validity of the Debye–Hückel approximation in EO, this Joule heating effect is essentially that due to the electric field, because of the very low velocities, so Eq. (6.35) reduces to $\dot{q} = \sigma\mathbf{E}\cdot\mathbf{E}$.

In principle, all fluid properties may depend on temperature and this strongly couples the rheological equation of state and the momentum equation on one side, with the thermal energy equation on the other. There are obvious advantages in considering fluid properties independent of temperature, because the fluid dynamics becomes independent of the thermal energy, simplifying the problem. The thermal energy equation, however, is always coupled with the flow via the velocity field and its gradients; therefore it can never be dealt with independently from the momentum equation.

6.5
Passive Mixing for Viscoelastic Fluids: Purely Elastic Flow Instabilities

6.5.1
General Considerations

As discussed in Section 6.1, the small length scales of microfluidics increase significantly the role of fluid elasticity beyond what can be achieved at the macroscale, and major differences in behavior are expected [1]. Indeed, complex flows of complex fluids often generate flow instabilities, even under inertialess (or creeping) flow conditions (i.e., when $Re \ll 1$), which are typically encountered at the microscale. These are called purely elastic flow instabilities and can play an important role in the context of mixing improvement at the microscale in viscoelastic fluid flows. In this section, we present an overview of elastic flow instabilities and focus on practical examples related to their development and enhancement at the microscale. As discussed in Section 6.1, flows at the microscale can be driven mainly by imposed pressure gradients, which are considered in this section, or using electrokinetic effects, which are considered in Section 6.6.

6.5.2 The Underlying Physics

The remarkable properties of complex fluids arise from the interaction between their molecular structure and the flow. The flow conditions induce a local molecular rearrangement, with the polymer chains being stretched and oriented. This nonequilibrium configuration generates large anisotropic normal stresses, which themselves influence the flow field. This feedback mechanism can lead to flow destabilization, and is more pronounced above the so-called coil–stretch transition that occurs when the strain rate exceeds half the inverse of the molecular relaxation time ($\dot{\varepsilon} \sim 1/2\lambda$). Under these conditions, the polymer molecules experience a transition from the coiled (equilibrium) configuration, to almost full extension.

The onset of elastic instabilities at high Wi is a hallmark of viscoelastic fluids, even under creeping flow conditions. Such purely elastic instabilities have been observed experimentally in a number of flow geometries, such as Taylor–Couette, cone-and-plate, contraction, and lid-driven cavity flows, among others [86, 121, 122]. For a thorough overview of purely elastic instabilities in (shear-dominated) viscometric flows, see the review paper by Shaqfeh [123].

Currently, it is widely accepted that the underlying mechanism for the onset of purely elastic instabilities in shear flows is related to streamline curvature, and the development of large hoop stresses, which generates tension along fluid streamlines leading to flow destabilization [86, 121, 122]. Pakdel and McKinley [86, 124] showed that the critical conditions for the onset of elastic instabilities can be described for a wide range of flows by a single dimensionless parameter, M, which accounts for elastic normal stresses and streamline curvature in the form

$$\sqrt{\frac{\lambda U}{\Re}\frac{\tau_{11}}{\tau_{12}}} \equiv M \geq M_{\text{crit}} \tag{6.36}$$

where λ is the relaxation time of the fluid, U is the local streamwise fluid velocity, τ_{11} is the local tensile stress in the flow direction, τ_{12} is the shear stress ($\tau_{12} = \eta\dot{\gamma}$), and $\Re$ is the streamline local radius of curvature. When the flow conditions are such that M locally exceeds a critical value, M_{crit}, elastic instabilities develop, as discussed by Pakdel and McKinley [86, 124] for several flow configurations. The value of M_{crit} is slightly dependent on the flow, and for simple flows, where the radius of curvature is known, M_{crit} can be estimated. As discussed by McKinley *et al.* [122], for Taylor–Couette flow $M_{\text{crit}} \approx 5.9$ and for torsional flow in a cone-and-plate arrangement, $M_{\text{crit}} \approx 4.6$. For more complex flows, the spatial variation of M needs to be taken into account to identify the critical regions where the largest value of M occurs. This mechanism for the onset of purely elastic instabilities and the applicability of the M parameter to identify the critical conditions for the onset of elastic instabilities was confirmed numerically by Alves and Poole [125] for creeping flow of UCM fluids in smooth contractions, for a wide range of contraction ratios.

6.5.3
Viscoelastic Instabilities in Some Canonical Flows

Purely elastic flow instabilities at the microscale have been observed experimentally and predicted numerically in several geometrical arrangements, such as those illustrated in Figure 6.10. The flows have been categorized in four main groups: (i) contraction/expansion flows; (ii) flows with interior stagnation points; (iii) wavy channels; and (iv) other flows. In all cases, the onset of the instability can be linked to the ubiquitous presence of large normal stresses and streamline curvature in shear dominated flows (e.g., wavy channels), extensional dominated flows (e.g., stagnation/flow focusing devices), or mixed kinematic flows (e.g., contraction/expansions).

Perhaps the most widely studied configuration associated to viscoelastic fluid flow is the contraction geometry. In fact, viscoelastic flow in contraction geometries has been the subject of numerous investigations (e.g., [126, 127]). Despite relying on a simple geometrical arrangement, contraction flows usually lead to complex flow patterns, which are very sensitive to the rheological properties of the fluid, and in

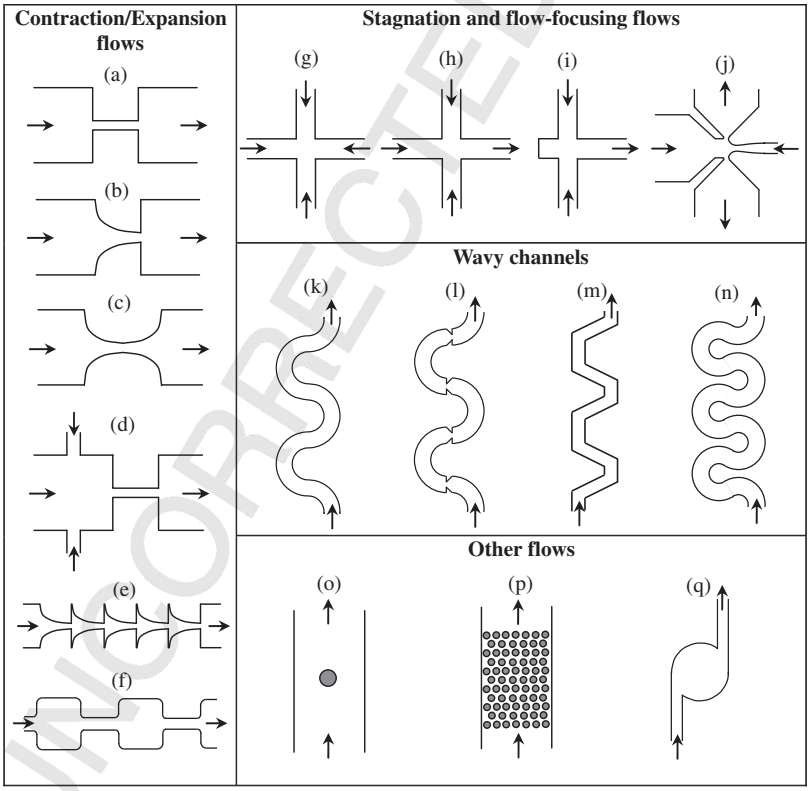

Figure 6.10 Sketch of several canonical geometrical arrangements investigated at the microscale using complex fluids that generate purely elastic flow instabilities.

particular to their extensional viscosity, geometrical details (e.g., significant differences of flow patterns are observed simply by rounding the re-entrant corner [128–130]), or the contraction ratio [131–133]. Due to their complex nature and geometrical simplicity, viscoelastic flows in abrupt contractions were established as one of the benchmark flow problems in computational rheology, during the *Vth International Workshop on Numerical Methods for Non-Newtonian Flows* [134], and since then they have been thoroughly investigated experimentally and numerically [127, 135–137]. Recent predictions of creeping flow in a 4: 1 planar contraction using the Oldroyd-B model were able to reproduce the main flow features and instabilities observed experimentally in contraction flows, up to the quasi-chaotic flow observed at high Weissenberg numbers [138].

Viscoelastic flows in microscale contractions/expansions have emerged in the past decade, after the pioneering work by McKinley and co-authors [51, 139]. Microscale contraction–expansion geometries (cf. Figure 6.10a–c) enable the exploration of previously unattained regions in the *Wi*–*Re* parameter space [139], and highly elastic flow conditions can be achieved even for dilute polymer solutions as illustrated in Figure 6.3. This opens the possibility of investigating the rheology of dilute polymer solutions, particularly if hyperbolic contractions are used, as illustrated in Figure 6.10b and c, which generate a nearly constant strain rate along the centerline [61, 66]. Interestingly, the instabilities promoted at highly elastic flow conditions provide a means to enhance mixing at the microscale, as demonstrated in the experiments of Rodd *et al.* [51] for simple abrupt contraction/expansions and extensively investigated by Gan *et al.* [53, 140] and Lam *et al.* [141] who patented a modified contraction/expansion microgeometry, shown in Figure 6.10d, with additional transverse streams to trigger the instability. This microfluidic contraction/expansion device was demonstrated to work efficiently for mixing purposes at low *Re* and can be used with biocompatible (viscoelastic) fluids, such as polyethylene oxide (PEO) polymer solutions [142].

Viscoelastic fluid flow in contractions is usually associated with enhanced pressure drop at large *Wi*, when the extensional viscosity of the working fluid has a strain-hardening behavior. The different strain histories experienced in smooth contraction/abrupt expansions and abrupt contraction/smooth expansions lead to anisotropic flow resistance and can be used to develop diode-like fluidic elements, as done by Groisman and Quake [49], who used a microfluidic device consisting of a series of connected triangular elements. For the same pressure gradient applied in each direction, they achieved flow rate ratios of about 2. More recently, Sousa *et al.* [52] proposed a modified design of the microfluidic device, consisting of a series of hyperbolic elements, as in Figure 6.10e. The pressure drop in the flow direction shown in Figure 6.10e was found to be more than four times higher than the pressure drop in the opposite direction, at the same flow rate, making such a microfluidic device suitable as a fluidic equivalent of an electronic diode. The enhanced flow resistance observed in such device was found to be linked with the onset of purely elastic flow instabilities, since the corresponding purely viscous Newtonian fluid flow showed no rectification effect at these low *Re*. The unsteady flow of viscoelastic fluids generated at high *Wi* can also be used to promote efficient mixing at low *Re* flow conditions.

The strong extensional flow generated in microcontraction/expansions and the large strain rates that can be achieved (of about $10^5\,s^{-1}$, or higher) make this geometrical configuration particularly interesting to study the stretching of long molecules, and in particular of DNA, under strong extensional fields. Following this idea, Gulati *et al.* [38] investigated the flow of semidilute solutions of λ-DNA in a 2 : 1 abrupt planar microcontraction at small *Re* (below 0.1) and high *Wi* (up to 629), corresponding to large elasticity numbers. Significant vortex enhancement was observed, particularly at high *Wi*, due to the highly elastic flow conditions. More recently, Hemminger *et al.* [143] investigated the flow of entangled DNA solutions, at different concentrations, using a 4 : 1 abrupt planar microcontraction. An unusual time-dependent shear banding flow was observed at the contraction entrance for the highest concentrations. Besides these important studies involving dilute and entangled DNA solutions, flow visualizations of the stretching and relaxation processes of individual DNA molecules in a microfluidic cross-slot geometry (cf. Figure 6.10g) have been done by Perkins *et al.* [144, 145], among others. The dynamics of single DNA molecules in post-arrays, as those illustrated in Figure 6.10p, have been investigated experimentally and numerically by Teclemariam *et al.* [146], showing that an appropriate design of post-array distribution controls DNA conformation and guides the location where the hooking events take place. A thorough review of the dynamics of a single DNA molecule in flow was presented by Shaqfeh [36].

Viscoelastic flows at high *De* (or high *Wi*) also exhibit purely elastic flow asymmetries in perfectly symmetric geometries. This steady symmetric to steady asymmetric flow transition was observed experimentally in the flow in a microscale cross-slot geometry [147] and were qualitatively captured by the 2D numerical simulations of Poole *et al.* [148] using the UCM model. Figure 6.11 displays a set of flow patterns predicted in the cross-slot geometry under creeping flow conditions for the UCM model for a range of *De* values. The Deborah number was defined as $De = \lambda U/H$ [148], where U is the average velocity on each arm of the cross-slot, with width H, as sketched in Figure 6.11. The numerical results are in qualitative agreement with the experiments of Arratia *et al.* [147] and show a progressive increase in the steady asymmetry above a critical Deborah number, $De_{crit} \approx 0.31$. At higher flow rates, a second instability sets in, at $De \approx 0.5$, and the flow becomes time-dependent. At significantly higher flow rates, the amplitude of oscillations increases and the flow eventually becomes chaotic, with a good mixing performance as measured by Arratia *et al.* [147].

Other extension-dominated flows have shown similar flow bifurcations and instabilities, as observed in the mixing–separating geometry [149], the six-arms 3D cross-slot [150], the flow-focusing device [54] (Figure 6.10h), the microfluidic T-junction geometry [55] (Figure 6.10i), or the *flip–flop* microfluidic device [48] (Figure 6.10j). For all these cases, the steady asymmetric instability occurs when large normal stresses are generated and with its onset a progressive transition from an extensionally dominated flow to a shear flow is observed to take place. This is shown in Figure 6.12 for a flow-focusing device, where the streamline patterns are superimposed onto the contour plots of the flow-type parameter, $\xi \equiv (1-R)/(1+R)$;

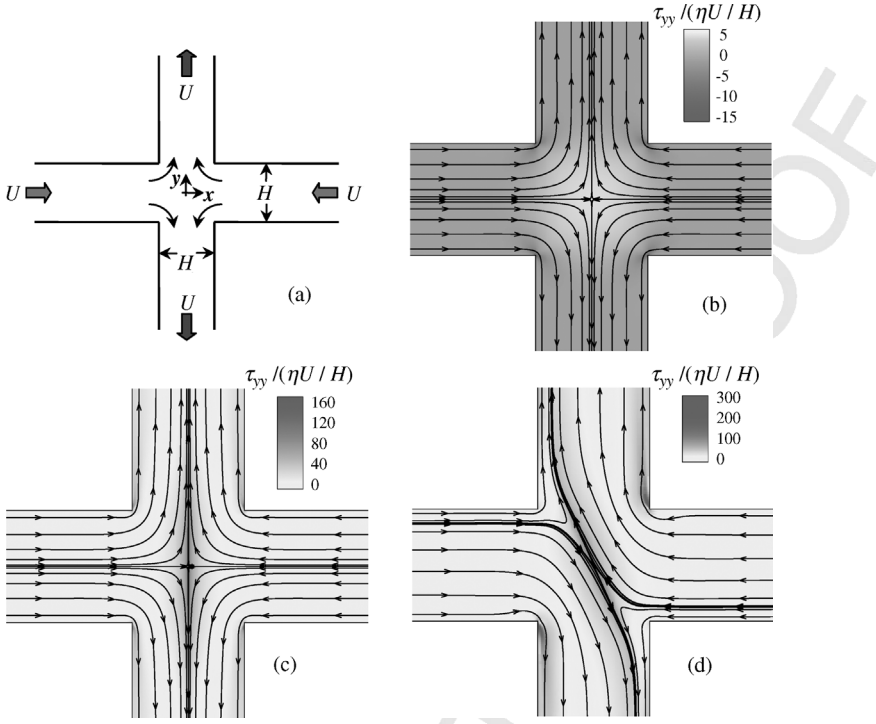

Figure 6.11 (a) Sketch of the cross-slot geometry. Streamline patterns predicted under creeping flow conditions for (b) a Newtonian fluid, and a UCM model at (c) $De = 0.3$ and (d) $De = 0.5$. The contours in (b–d) represent the normalized normal stress, $\tau_{yy}/(\eta U/H)$. Adapted from [148].

with $R = \mathrm{tr}(\mathbf{W}^2)/\mathrm{tr}(\mathbf{D}^2)$, where $\mathbf{W}$ is the relative rate of rotation tensor and $\mathbf{D}$ is the strain-rate tensor [151]. This invariant is illustrated in Figure 6.12 and varies from $\xi = -1$, corresponding to solid-like rotation flow, up to $\xi = 1$, corresponding to pure extensional flow. Shear flow corresponds to $\xi = 0$ and is easily identified near the walls, and along the channels under fully developed flow conditions.

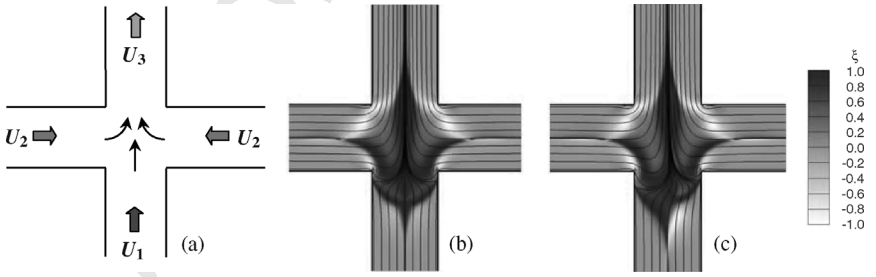

Figure 6.12 Extensional flow of a UCM fluid in a flow focusing microgeometry under creeping flow conditions. (a) Sketch of the geometry; (b) $De = 0.3$; (c) $De = 0.34$. Adapted from [54].

Despite the success in the prediction of elastic-driven steady asymmetric flow instabilities, the underlying mechanisms are yet to be fully understood, particularly the cascade of events from the first "well-behaved simple" transition to the quasi-chaotic behavior observed at very high *Wi*. In fact, a significantly more complex elastic instability, also not yet fully understood, is the phenomenon of elastic turbulence which also occurs for creeping flow conditions. The transition to turbulence at extremely small *Re* was reported for the first time by Groisman and Steinberg [88] for torsional flow of a dilute solution of a high-molecular-weight polyacrylamide between two parallel disks. In the elastic turbulence regime, despite the Reynolds number being arbitrarily small, the hallmark characteristics of classical turbulence at high *Re* are observed, such as enhanced flow resistance, enhanced mass and heat transfer rates, enhanced mixing, and a wide range of temporal and spatial fluctuations, as demonstrated in several subsequent experimental studies (e.g., [87, 152]), including the torsional flow between parallel plates or the flow in a wavy channel (with a square section of $3 \times 3\ \text{mm}^2$, so not in the microfluidic range), as sketched in Figure 6.10k. Other investigations at the microscale involving wavy channels include the work of Groisman *et al*. [48] using a channel with a similar shape to that in Figure 6.10l. When using polymer solutions, such microfluidic devices work as the fluidic equivalent of a nonlinear resistor, producing a nearly constant flow rate for a wide range of pressure drops across the channel. Other studies involving zigzag channels and dilute polymer solutions showed the good mixing properties that can be achieved at high *Wi*, due to the onset of elastic instabilities [50] (Figure 6.10m). In contrast, for Newtonian fluids, a decrease in the mixing performance is observed when the flow rate is increased, due to the reduction in mixing time, which for low *Re* Newtonian flows is mainly induced by diffusion. Recently, Li *et al*. [153] used surfactant solutions with viscoelastic behavior (cetyltrimethyl ammonium chloride/sodium salicylate, CTAC/NaSal) and observed the onset of chaotic motion in three types of microchannels that include curved streamlines, such as wavy channels (Figure 6.10n), flow past a confined cylinder in a rectangular microchannel (Figure 6.10o), and flow in a round microfluidic cavity (Figure 6.10q). Again, the viscoelasticity of the surfactant solution together with the curved streamlines were responsible for the onset of elastic instabilities, leading to chaotic behavior and generating enhanced mixing for elastic turbulence flow conditions.

6.5.4 Elastic Turbulence

The transition to elastic turbulence depends strongly on the strain history experienced by the fluid, which is induced by the shape of the flow geometry, and on the rheological properties of the polymer solution. Nevertheless, using polymer solutions with sufficiently high elasticity, one expects that this turbulent-like motion can be excited at arbitrarily low velocities and in arbitrarily small geometries, even for very dilute polymeric solutions [154]. The elasticity of the flow increases with the inverse of the square characteristic length scale of the flow geometry (cf. Eq. (6.4)) and consequently, in microscale flows adding minute amounts of long molecules

to the solution (on the order of 10 ppm, or above), is usually sufficient to induce non-Newtonian behavior at large deformation rates, which are typical of microscale flows [52, 87, 155].

So far, most of the works concerning elastic turbulence have been primarily experimental [87, 88, 152, 154, 156], and theoretical [155, 157]. The numerical simulation of elastic-driven flow instabilities has been restricted to the initial phases of flow transitions [125, 138, 148]. Only recently some preliminary attempts to simulate the elastic turbulence regime have been successful, for simplified 2D flow arrangements, such as the periodic Kolmogorov shear flow with constant forcing [158, 159]. Using direct numerical simulations (DNS) and the Oldroyd-B model to describe the fluid rheology, these authors demonstrated the occurrence of flow destabilization induced by the elastic forces due to the dynamics of polymer molecules in the solution. At large *Wi*, the basic phenomenology found in experimental studies of elastic turbulence was reproduced in this idealized geometrical configuration, with the appearance of coherent structures in the form of "elastic waves" [159]. Despite the use of an idealized geometrical configuration with the corresponding limitations, namely the assumption of 2D flow, Berti and Boffetta [159] demonstrated that the use of simple viscoelastic models, such as the Oldroyd-B constitutive equation, can capture the essential features of elastic turbulence, opening a window to more realistic simulations using real 3D microfluidic flow geometries and more adequate constitutive equations.

Much more needs to be investigated regarding the progressive transitions to elastic turbulence and this must be accomplished experimentally, using fluids of well-controlled rheology, and complemented with computational and theoretical studies for better insight of the complex underlying mechanisms of flow instabilities. Although there are important similarities between inertial and elastic turbulence, this does not imply that the underlying physical mechanism is the same in both cases. Indeed, elastic turbulence is accompanied by significant stretching of the polymer molecules, which is the main cause of the observed increase in the elastic normal stresses and the inherent increase in flow resistance, a ubiquitous characteristic of turbulence. The stretching of the molecular chains leads to a strong increase in flow resistance due to the increase in the extensional viscosity, a characteristic of long macromolecules in extensional flow [45], very much like the production of large Reynolds stresses in inertial turbulence of Newtonian fluids, but contrasting with the severe damping of the same Reynolds stresses that accompany polymer-induced drag reduction in high *Re* inertial turbulence. Understanding the nature and mechanisms that lead to elastic turbulence will have important practical applications, either for enhancing mixing and/or heat and mass transfer rates at the microscale, or for allowing the operation of extrusion processes at higher throughputs, by minimizing the driving forces that lead to the onset of flow instabilities. Additionally, understanding the driving mechanisms of elastic turbulence and comparison with classical inertial-driven turbulence of Newtonian fluids may allow us to obtain further insights into the driving mechanisms of inertial turbulence in Newtonian and in viscoelastic fluid flows.

6.6 Other Forcing Methods

The previous section discussed instabilities at high *Wi* flows of complex fluids driven by a pressure gradient. Here we briefly describe important works that use electrokinetic forcing to promote complex fluid flow, with emphasis on EO and electrophoresis. EOF are important in the context of viscoelastic fluids, including the development of instabilities and their possible application in micromixing enhancement. To finalize this chapter, electrophoresis is also considered, not in the framework of mixing, but rather because of its importance in the limiting case of the manipulation and separation of individual macromolecules, and of its close link with EO.

6.6.1 Electro-Osmosis

Currently, about 90% of microfluidic devices operate by either pressure-driven or EOF forcing, essentially due to their versatility and simplicity of operation [160]. PDF are still leading the number of applications of microfluidics; however as the size of the microchannels is further reduced, say to dimensions below around 10 μm, forcing by pressure becomes particularly inefficient due to the significant increase in viscous losses [160]. In contrast, for this range of dimensions EO becomes a particularly convenient and efficient way of promoting flow in microfluidic devices, as long as the fluid has ions. A major disadvantage of EOF is the strong electric gradients that typically need to be applied to promote the flow at average velocities above $1\,\mathrm{mm\,s^{-1}}$. This limitation can be circumvented by further miniaturization, thus making EOF more efficient as the size is reduced, with important applications in nanofluidics where smaller electrical potentials are sufficient to promote the flow. A thorough discussion on the advantages and disadvantages of PDF and EOF is presented in [160].

Rigorous modeling of EOF in microchannels has been the subject of several studies, particularly for Newtonian fluids. A thorough review with various applications of EO is presented in [58, 161]. Exact analytical solutions have been derived under fully developed flow conditions for Newtonian fluids, as described by Afonso *et al.* [162]. Newtonian fluid flow in complex geometries has been modeled in several works, and accurate results have been obtained for different applications. Of particular interest are electrokinetic instabilities (EKI) that arise under high electric fields in the presence of electrical conductivity gradients. Electrokinetic flows of Newtonian fluids become unstable when electroviscous advection of conductivity fields dominates over dissipation through viscosity and molecular diffusion [163, 164]. Likewise, EKI can be triggered using time-periodic fields, as demonstrated by Shin *et al.* [165] using a flow-focusing device (Figure 6.10h).

Surface patterning with different materials has been exploited to generate regions with different zeta potentials, and chaotic mixing in EOF can be driven by spatiotemporal surface charge modulation [166]. Other examples of nonlinear

electrokinetic phenomena with great potential in microfluidics mixing and pumping are induced-charge electro-osmosis (ICEO) and AC electro-osmosis (ACEO), as reviewed by Bazant and Squires [167].

In contrast, EOF of complex fluids are still poorly studied, except for fully developed flows between parallel plates and in a circular tube, thus constituting a fertile ground for research. The theoretical study of EO flows of non-Newtonian fluids is recent and the preliminary works considered GNF, such as the power-law model [168, 169]). Berli and Olivares [170] considered the existence of a small wall layer depleted of additives (the skimming layer), in which the fluid behaves as a Newtonian fluid, and the non-Newtonian behavior is restricted to the electrically neutral region outside the EDL. More recently, the theoretical analysis of EO flows was extended to viscoelastic fluids by Park and Lee [171], who derived the Helmholtz–Smoluchowski velocity for pure EOF of PTT fluids in rectangular channels and provided a simple numerical procedure for its calculation. Afonso *et al.* [162] considered the PTT and FENE-P constitutive equations, and derived analytical expressions for fully developed flow between parallel plates and in a circular pipe, under combined pressure and electrokinetic forcings. This analysis was extended by Afonso *et al.* [172] to consider different zeta potentials on both walls, whereas Sousa *et al.* [173] considered the existence of a skimming layer near the wall depleted of polymer molecules.

EOF of polymer solutions have also been studied experimentally in simple geometries. Bello *et al.* [174] investigated the flow of polymer solutions in capillaries, and observed a progressively suppressed EOF, suggesting a dynamic coating of the polymer molecules onto the capillary wall. Baumler *et al.* [175] and Chang and Tsao [176] observed drag reduction in EOF of polymer solutions, due to polymer depletion in the EDL, which leads to a reduction in shear viscosity with corresponding enhancement of the measured Helmholtz–Smoluchowski velocity.

High Weissenberg number flows are prone to purely elastic instabilities, as discussed in the previous section. EOF of polymer solutions are no exception, and Dhinakaran *et al.* [118] predicted a constitutive-related instability for EO flow between parallel plates of PTT fluids, when the shear rate exceeds a critical value. Purely elastic instabilities can also be generated in EO flows, and such electroelastic instabilities were recently observed experimentally in a microfluidic channel consisting of a series of 2 : 1 sudden contraction/expansions (Figure 6.10f), using dilute viscoelastic PAA solutions [177, 178]. EOF are an excellent platform to generate strong extensional flows because shear effects are typically circumscribed to the EDL region. The experimental results of Bryce and Freeman [177, 178] suggest that the electroelastic instability occurs for flow conditions corresponding to the coil–stretch transition, without the observation of a dominant frequency of the flow, an indication of chaotic-like behavior. Despite this unstable behavior, the mixing rates found were smaller than those observed in polymer-free solutions, with diffusion appearing to be the dominant mixing mechanism [177]. This is a surprising result, and further investigations of electroelastic instabilities are required to enlighten the mechanism of purely elastic instabilities and mixing in microfluidic EO flows of polymer solutions.

6.6.2 Electrophoresis

In many ways, DNA can be considered as an ideal model polymer. It is naturally monodisperse, large enough to be imaged in a microscope using fluorescence techniques, and ~~the~~ relaxation time is typically of the order of seconds [179]. DNA is a polyelectrolyte, making it easy to be manipulated through electrophoresis by applying electric fields. We note, however, that the (micro)fluidic channels used usually have charged surfaces, which also induce a global transport through EO, unless special treatments are applied to the surfaces to minimize electro-osmotic transport [180].

In a strict sense, electrophoresis is usually not included in the field of rheology. However, since it involves deformation and flow of matter, albeit in a single molecule framework, this tacit distinction is becoming obsolete, with experiments using biopolymers progressively creating an important influence on rheology [179]. Likewise, some tools developed for microrheology are expected to be increasingly used in the manipulation of single DNA molecules. A growing interaction between rheology and biophysics is leading to important insights into the flow properties of polymers and biomolecules [181]. Electrophoresis of macromolecules has several applications in molecular biology, including the transport, separation, or elongation at the molecular level, with important applications in biotechnology and medicine, with DNA sequencing being one of the most prominent. A recent review of electrophoretic microfluidic separation techniques was presented by Wu *et al*. [182], summarizing important milestones in the separation of small molecules, DNA, and proteins.

Specific microfluidic devices have been proposed and optimized in order to study individual molecules, and DNA in particular. Stretching of DNA molecules is a key technology in emerging DNA-mapping devices such as direct linear analysis [183], and single-molecule studies of DNA have expanded our knowledge on the fundamentals of polymer physics. Additionally, understanding the response of individual polymers at the molecular level can provide valuable information to develop models applicable to entangled systems. Electrophoresis stretching and relaxation of DNA molecules have been undertaken in several flow configurations that promote a strong extensional field, such as hyperbolic contractions, cross–slot, and T-junction arrangements. Juang *et al*. [184] used a cross-slot microfluidic channel to induce a fairly homogeneous 2D elongational flow, allowing the determination of the amount of DNA stretching. Kim and Doyle [183] used hyperbolic contractions, which generate a nearly constant strain rate, with additional lateral streams to enhance DNA stretching. Balducci and Doyle [185] also used hyperbolic contractions, but included an obstacle array upstream of the contraction region for conformational preconditioning, leading to an increase in the average deformation of the DNA molecule in the contraction. Tang and Doyle [186] proposed a microfluidic T-shaped channel which can trap and significantly stretch single DNA molecules using electrophoresis, without requiring any special end functionalization to trap the DNA molecule.

The relaxation process of DNA is also of interest as it allows for the determination of the molecular relaxation time, which is an important parameter for the characterization of DNA dynamics as shown in several experimental studies [187–189].

6.7 Conclusions and Perspectives

Flow systems built around microfluidics are becoming increasingly popular in a wide range of industrial applications dealing with both gas and liquids. They associate low production costs with low power consumption and waste reduction, allow for easy integration with electronics toward the lab-on-chip devices, but require demanding manufacturing facilities and highly efficient signal detection systems. Many of their applications are in biotechnology and in health related areas, where the liquids are made of complex structures and macromolecules that impart nonlinear rheological behavior and in particular viscoelasticity. Since microscale flows are characterized by high surface-to-volume ratios, the flow dynamics is significantly affected by fluid rheology and other physical phenomena, such as surface tension, in comparison with macroscale flows. In particular, the time scale of the flows, $t_f \sim L/U$, decreases significantly to become much smaller than (or at least on the order of) the relaxation time of the fluid structures, keeping the flow Reynolds number small. As a consequence, microscale flows of complex fluids are characterized by large elastic effects in comparison to the corresponding Newtonian flows and both exhibit large ratios of viscous to inertial forces, in contrast to the corresponding macroscale flows dominated by inertia.

The large elastic effects found in microfluidic flows of complex fluids allow for enhanced mixing due to purely elastic instabilities, which are a consequence of the nonlinear nature of the corresponding terms of the rheological constitutive equation. In fact, the onset of elastic instabilities has been found to take place over a wide range of flow types (flows dominated by extension or shear, as well as flows having mixed kinematics), whenever there are large normal stresses of elastic origin coupled with streamline curvature. The dynamics of these instabilities, which exist even in the limit of creeping flow, do have some resemblance to inertial instabilities found in high Reynolds number flows of Newtonian fluids, in the sense of a progressive cascade of instabilities from simple transitions between steady flows to transitions to periodic unsteady and subsequently chaotic flows leading eventually to elastic turbulence, where the unstable flow structures exist over a continuous wide range of length and time scales. The path of these transitions is only now being discovered and remains an active topic of research. The onset of elastic turbulence in regions of parallel shear flow is currently particularly challenging.

The presence of macromolecules in microscale flow systems thus allows for enhanced mixing in low Reynolds number flows via elasticity-driven instabilities. These not only exist in pressure-gradient driven flows, but also for electrically driven flows, which are potentially very useful given their ease of implementation at these scales. The combination of EO with viscoelasticity is a new topic of research, where

most things remain to be done and it suffices to think here that it is not only direct but also alternate current that has to be considered. Additionally, electrokinetic effects can be combined with surface patterning, which can also be used to enhance other surface phenomena, such as the generation of surface tension gradients. Their combination with complex fluids is in its infancy and is certainly worth exploring to find possible and unexpected flow features and applications.

Acknowledgments

The authors acknowledge funding by FEDER and Fundação para a Ciência e a Tecnologia over the last 6 years through projects REEQ/262/EME/2005, REEQ/928/EME/2005, POCI/EME/59338/2004, PTDC/EME-MFE/70186/2006, PTDC/EQU-FTT/70727/2006, ~~and~~ PTDC/EQU-FTT/71800/2006.

References

1 Squires, T.M. and Quake, S.R. (2005) Microfluidics: Fluid physics at the nanoliter scale. *Reviews of Modern Physics*, **77**, 977–1026.
2 Whitesides, G.M. (2006) The origins and the future of microfluidics. *Nature*, **442**, 368–373.
3 Saville, D.A. (1977) Electrokinetic effects with small particles. *Annual Review of Fluid Mechanics*, **9**, 321–337.
4 Probstein, R.F. (2003) *Physicochemical Hydrodynamics, an Introduction*, 2nd edn, Wiley-Interscience, Hoboken, NJ.
5 Gad-el-Hak, M.G. (2002) *The MEMS Handbook*, CRC Press, Boca Raton, FL.
6 Bruus, H. (2008) *Theoretical Microfluidics, Oxford Master Series in Condensed Matter Physics*, Oxford University Press, Oxford, UK.
7 Ajdari, A. (2000) Pumping liquids using asymmetric electrode arrays. *Physical Review E*, **61**, R45–R48.
8 Bazant, M.Z. and Squires, T.M. (2004) Induced-charge electrokinetic phenomena: Theory and microfluidic applications. *Physical Review Letters*, **92**, 066101.
9 Stone, H.A., Stroock, A.D., and Ajdari, A. (2004) Engineering flows in small devices: microfluidics toward lab-on-a-chip. *Annual Review of Fluid Mechanics*, **36**, 381–411.
10 Laser, D.J. and Santiago, J.G. (2004) A review of micropumps. *Journal of Micromechanics and Microengineering*, **14**, R35–R64.
11 Stone, H.A. (2009) Microfluidics, tuned-in flow control. *Nature Physics*, **5**, 178–179.
12 Brody, J.P., Kamholz, A.E., and Yager, P. (1997) Prominent microscopic effects in microfabricated fluidic analysis systems. Micro- and Nanofabricated Electro-Optical Mechanical Systems for Biomedical and Environmental Applications, Proceedings of, **2978** pp. 103–110.
13 Hatch, A., Kamholz, A.E., Hawkins, K.R., Munson, M.S., Schilling, E.A., Weigl, B.H., and Yager, P. (2001) A rapid diffusion immunoassay in a T-sensor. *Nature Biotechnology*, **19**, 461–465.
14 Dendukuri, D., Tsoi, K., Hatton, T.A., and Doyle, P.S. (2005) Controlled synthesis of nonspherical microparticles using microfluidics. *Langmuir*, **21**, 2113–2116.
15 Nguyen, N.-T. (2008) *Micromixers: Fundamentals, Design and Fabrication*, William Andrew, Norwich, NY.
16 Sia, S.K. and Whitesides, G.M. (2003) Microfluidic devices fabricated in poly (dimethylsiloxane) for biological studies. *Electrophoresis*, **24**, 3563–3576.

17 Pittet, P., Lu, G.N., Galvan, J.M., Ferrigno, R., Stephan, K., Blum, L.J., and Leca-Bouvier, B. (2008) A novel low-cost approach of implementing electrochemiluminescence detection for microfluidic analytical systems. *Materials Science & Engineering C-Biomimetic and Supramolecular Systems*, **28**, 891–895.

18 Kallio, P. and Kuncova, J. (2004) Microfluidics. *Technology Review*, **158**, 2004.

19 Nguyen, N.T. and Wu, Z.G. (2005) Micromixers – a review. *Journal of Micromechanics and Microengineering*, **15**, R1–R16.

20 Oh, K.W. and Ahn, C.H. (2006) A review of microvalves. *Journal of Micromechanics and Microengineering*, **16**, R13–R39.

21 Quake, S.R. and Scherer, A. (2000) From micro- to nanofabrication with soft materials. *Science*, **290**, 1536–1540.

22 Ng, J.M.K., Gitlin, I., Stroock, A.D., and Whitesides, G.M. (2002) Components for integrated poly(dimethylsiloxane) microfluidic systems. *Electrophoresis*, **23**, 3461–3473.

23 Marrian, C.R.K. and Tennant, D.M. (2003) Nanofabrication. *Journal of Vacuum Science & Technology A – Vacuum Surfaces and Films*, **21**, S207–S215.

24 Bayraktar, T. and Pidugu, S.B. (2006) Characterization of liquid flows in microfluidic systems. *International Journal of Heat and Mass Transfer*, **49**, 815–824.

25 Whitesides, G.M. and Stroock, A.D. (2001) Flexible methods for microfluidics. *Physics Today*, **54**, 42–48.

26 Thorsen, T., Roberts, R.W., Arnold, F.H., and Quake, S.R. (2001) Dynamic pattern formation in a vesicle-generating microfluidic device. *Physical Review Letters*, **86**, 4163–4166.

27 Anna, S.L., Bontoux, N., and Stone, H.A. (2003) Formation of dispersions using "flow focusing" in microchannels. *Applied Physics Letters*, **82**, 364–366.

28 Yang, T.L., Jung, S.Y., Mao, H.B., and Cremer, P.S. (2001) Fabrication of phospholipid bilayer-coated microchannels for on-chip immunoassays. *Analytical Chemistry*, **73**, 165–169.

29 Fu, A.Y., Spence, C., Scherer, A., Arnold, F.H., and Quake, S.R. (1999) A microfabricated fluorescence-activated cell sorter. *Nature Biotechnology*, **17**, 1109–1111.

30 Sohn, L.L., Saleh, O.A., Facer, G.R., Beavis, A.J., Allan, R.S., and Notterman, D.A. (2000) Capacitance cytometry: Measuring biological cells one by one. *Proceedings of the National Academy of Sciences of the United States of America*, **97**, 10687–10690.

31 Chiu, D.T., Jeon, N.L., Huang, S., Kane, R.S., Wargo, C.J., Choi, I.S., Ingber, D.E., and Whitesides, G.M. (2000) Patterned deposition of cells and proteins onto surfaces by using three-dimensional microfluidic systems. *Proceedings of the National Academy of Sciences of the United States of America*, **97**, 2408–2413.

32 Li, J.J., Kelly, J.F., Chemushevich, I., Harrison, D.J., and Thibault, P. (2000) Separation and identification of peptides from gel-isolated membrane proteins using a microfabricated device for combined capillary electrophoresis/nanoelectrospray mass spectrometry. *Analytical Chemistry*, **72**, 599–609.

33 Beebe, D.J., Mensing, G.A., and Walker, G.M. (2002) Physics and applications of microfluidics in biology. *Annual Review of Biomedical Engineering*, **4**, 261–286.

34 Zare, R.N. and Kim, S. (2010) Microfluidic platforms for single-cell analysis. *Annual Review of Biomedical Engineering*, **12**, 187–201.

35 Tegenfeldt, J.O., Prinz, C., Cao, H., Huang, R.L., Austin, R.H., Chou, S.Y., Cox, E.C., and Sturm, J.C. (2004) Micro- and nanofluidics for DNA analysis. *Analytical and Bioanalytical Chemistry*, **378**, 1678–1692.

36 Shaqfeh, E.S.G. (2005) The dynamics of single-molecule DNA in flow. *Journal of Non-Newtonian Fluid Mechanics*, **130**, 1–28.

37 Randall, G.C., Schultz, K.M., and Doyle, P.S. (2006) Methods to electrophoretically stretch DNA: Microcontractions, gels, and hybrid gel-microcontraction devices. *Lab on a Chip*, **6**, 516–525.

38 Gulati, S., Muller, S.J., and Liepmann, D. (2008) Direct measurements of viscoelastic flows of DNA in a 2: 1 abrupt planar micro-contraction. *Journal of Non-Newtonian Fluid Mechanics*, **155**, 51–66.

39 Choban, E.R., Markoski, L.J., Wieckowski, A., and Kenis, P.J.A. (2004) Microfluidic fuel cell based on laminar flow. *Journal of Power Sources*, **128**, 54–60.

40 Obot, N.T. (2002) Toward a better understanding of friction and heat/mass transfer in microchannels – A literature review. *Microscale Thermophysical Engineering*, **6**, 155–173.

41 Hansen, C. and Quake, S.R. (2003) Microfluidics in structural biology: smaller, faster... better. *Current Opinion in Structural Biology*, **13**, 538–544.

42 Gad-el-Hak, M. (2005) Liquids: The holy grail of microfluidic modeling. *Physics of Fluids*, **17**, 100612.

43 Breussin, F. (2009) Emerging markets for microfluidic applications in Life Sciences and In-Vitro Diagnostics, EMMA Report, Yole Dévelopment SA.

44 Tabeling, P. (2005) *Introduction to Microfluidics*, Oxford University Press, Oxford.

45 Bird, R.B., Armstrong, R.C., and Hassager, O. (1987) *Dynamics of Polymeric Liquids. Volume 1: Fluid Mechanics*, Wiley, New York.

46 Larson, R.G. (1999) *The Structure and Rheology of Complex Fluids*, Oxford University Press, Oxford.

47 Dealy, J.M. (2010) Weissenberg and Deborah numbers – Their definition and use. *Rheology Bulletin*, **79**, 14–18.

48 Groisman, A., Enzelberger, M., and Quake, S.R. (2003) Microfluidic memory and control devices. *Science*, **300**, 955–958.

49 Groisman, A. and Quake, S.R. (2004) A microfluidic rectifier: anisotropic flow resistance at low Reynolds numbers. *Physical Review Letters*, **92**, 094501-1–094501-4.

50 Pathak, J.A., Ross, D., and Migler, K.B. (2004) Elastic flow instability, curved streamlines, and mixing in microfluidic flows. *Physics of Fluids*, **16**, 4028-1–4028-7.

51 Rodd, L.E., Scott, T.P., Boger, D.V., Cooper-White, J.J., and McKinley, G.H. (2005) The inertio-elastic planar entry flow of low-viscosity elastic fluids in micro-fabricated geometries. *Journal of Non-Newtonian Fluid Mechanics*, **129**, 1–22.

52 Sousa, P.C., Pinho, F.T., Oliveira, M.S.N., and Alves, M.A. (2010) Efficient microfluidic rectifiers for viscoelastic fluid flow. *Journal of Non-Newtonian Fluid Mechanics*, **165**, 652–671.

53 Gan, H.Y., Lam, Y.C., and Nguyen, N.T. (2006) Polymer-based device for efficient mixing of viscoelastic fluids. *Applied Physics Letters*, **88**, 224103.

54 Oliveira, M.S.N., Pinho, F.T., Poole, R.J., Oliveira, P.J., and Alves, M.A. (2009) Purely-elastic flow asymmetries in flow-focusing devices. *Journal of Non-Newtonian Fluid Mechanics*, **160**, 31–39.

55 Soulages, J., Oliveira, M.S.N., Sousa, P.C., Alves, M.A., and McKinley, G.H. (2009) Investigating the stability of viscoelastic stagnation flows in T-shaped microchannels. *Journal of Non-Newtonian Fluid Mechanics*, **163**, 9–24.

56 Batchelor, G.K. (2000) *An Introduction to Fluid Dynamics*, Cambridge University Press, Cambridge, UK; New York, NY.

57 Nguyen, N.-T. and Wereley, S.T. (2006) *Fundamentals and Applications of Microfluidics*, 2nd edn, Artech House, Norwood.

58 Karniadakis, G., Beskok, A., and Aluru, N. (2005) *Microflows and nanoflows. Fundamentals and Simulation, Interdisciplinary Applied Mathematics Series*, vol. 29, Springer, Berlin.

59 Koo, J.M. and Kleinstreuer, C. (2003) Liquid flow in microchannels: experimental observations and computational analyses of microfluidics effects. *Journal of Micromechanics and Microengineering*, **13**, 568–579.

60 Sharp, K.V. and Adrian, R.J. (2004) Transition from laminar to turbulent flow in liquid filled microtubes. *Exp Fluids*, **36**, 741–747.

61 Oliveira, M.S.N., Alves, M.A., Pinho, F.T., and McKinley, G.H. (2007) Viscous flow through microfabricated hyperbolic

contractions. *Experiments in Fluids*, **43**, 437–451.
62 Oliveira, M.S.N., Rodd, L.E., McKinley, G.H., and Alves, M.A. (2008) Simulations of extensional flow in microrheometric devices. *Microfluid Nanofluid*, **5**, 809–826.
63 Pit, R., Hervet, H., and Leger, L. (2000) Direct experimental evidence of slip in hexadecane: Solid interfaces. *Physical Review Letters*, **85**, 980–983.
64 Barrat, J.L. and Bocquet, L. (1999) Large slip effect at a nonwetting fluid-solid interface. *Physical Review Letters*, **82**, 4671–4674.
65 Colin, S. (2005) Rarefaction and compressibility effects on steady and transient gas flows in microchannels. *Microfluid Nanofluid*, **1**, 268–279.
66 Pipe, C.J. and McKinley, G.H. (2009) Microfluidic rheometry. *Mechanics Research Communications*, **36**, 110–120.
67 Ottino, J.M. and Wiggins, S. (2004) Applied physics – Designing optimal micromixers. *Science*, **305**, 485–486.
68 Wang, H.Z., Iovenitti, P., Harvey, E., and Masood, S. (2002) Optimizing layout of obstacles for enhanced mixing m microchannels. *Smart Materials & Structures*, **11**, 662–667.
69 Brody, J.P., Yager, P., Goldstein, R.E., and Austin, RH. (1996) Biotechnology at low Reynolds numbers. *Biophysical Journal*, **71**, 3430–3441.
70 Ottino, J.M. (2004) *The Kinematics of Mixing: Stretching, Chaos, and Transport*, Cambridge University Press, Cambridge, UK.
71 Coleman, J.T. and Sinton, D. (2005) A sequential-injection microfluidic mixing strategy. *Microfluid Nanofluid*, **1**, 319–327.
72 Glasgow, I. and Aubry, N. (2003) Enhancement of microfluidic mixing using time pulsing. *Lab on a Chip*, **3**, 114–120.
73 Deshmukh, A.A., Liepmann, D., and Pisano, A.P. (2000) Continuous micromixer with pulsatile micropumps. Technical Digest of the IEEE Solid State Sensor and Actuator Workshop (Hilton Nead Island, SC) 73–76.
74 El Moctar, A.O., Aubry, N., and Batton, J. (2003) Electro-hydrodynamic micro-fluidic mixer. *Lab on a Chip*, **3**, 273–280.
75 Bau, H.H., Zhong, J., and Yi, M. (2001) A minute magneto hydro dynamic (MHD) mixer. *Sensors and Actuators B: Chemical*, **79**, 207–215.
76 Qian, S. and Bau, H.H. (2009) Magneto-hydrodynamics based microfluidics. *Mechanics Research Communications*, **36**, 10–21.
77 Yang, Z., Goto, H., Matsumoto, M., and Maeda, R. (2000) Active micromixer for microfluidic systems using lead-zirconate-titanate (PZT)-generated ultrasonic vibration. *Electrophoresis*, **21**, 116–119.
78 Yang, Z., Matsumoto, S., Goto, H., Matsumoto, M., and Maeda, R. (2001) Ultrasonic micromixer for microfluidic systems. *Sensor Actuators A – Phys*, **93**, 266–272.
79 Hessel, V., Lowe, H., and Schonfeld, F. (2005) Micromixers – a review on passive and active mixing principles. *Chemical Engineering Science*, **60**, 2479–2501.
80 Aref, H. (1984) Stirring by chaotic advection. *Journal of Fluid Mechanics*, **143**, 1–21.
81 Stroock, A.D., Dertinger, S.K.W., Ajdari, A., Mezic, I., Stone, H.A., and Whitesides, G.M. (2002) Chaotic mixer for microchannels. *Science*, **295**, 647–651.
82 Gleeson, J.P. (2005) Transient micromixing: Examples of laminar and chaotic stirring. *Physics of Fluids*, **17**, 100614.
83 Tadmor, Z. and Gogos, C.G. (2006) *Principles of Polymer Processing*, 2nd edn, Wiley-Interscience, Hoboken, NJ.
84 Oliveira, M.S.N., Pinho, F.T., and Alves, M.A. (2008) Extensional effects in viscoelastic fluid flow through a micro-scale double cross-slot. Xvth International Congress on Rheology – the Society of Rheology 80th Annual Meeting, Pts 1 and 2, 1027, pp. 982–984.
85 Townsend, P., Walters, K., and Waterhouse, W.M. (1976) Secondary flows in pipes of square cross-section and measurement of 2nd normal stress difference. *Journal of Non-Newtonian Fluid Mechanics*, **1**, 107–123.

86 Pakdel, P. and McKinley, G.H. (1996) Elastic instability and curved streamlines. *Physical Review Letters*, **77**, 2459–2462.

87 Groisman, A. and Steinberg, V. (2004) Elastic turbulence in curvilinear flows of polymer solutions. *New Journal of Physics*, **6–29**, 1–48.

88 Groisman, A. and Steinberg, V. (2000) Elastic turbulence in a polymer solution flow. *Nature*, **405**, 53–55.

89 Whorlow, R.W. (1992) *Rheological Techniques*, 2nd edn, Ellis Horwood Series in Physics and Its Applications, London.

90 Walters, K. (1975) *Rheometry*, Chapman and Hall, London.

91 Chen, D.C.-H. (1986) Yield stress: A time-dependent property and how to measure it. *Rheologica Acta*, **25**, 542–554.

92 Nguyen, Q.D. and Boger, D.V. (1992) Measuring the flow properties of yield stress fluids. *Annual Review of Fluid Mechanics*, **24**, 47–88.

93 Barnes, H.A. and Walters, K. (1985) The yield stress myth? *Rheologica Acta*, **24**, 323–326.

94 Barnes, H.A. (1995) A review of the slip (wall depletion) of polymer solutions, emulsions and particle suspensions in viscometers: its cause, character and cure. *Journal of Non-Newtonian Fluid Mechanics*, **56**, 221–251.

95 Barnes, H.A. (1999) The yield stress – a review or 'παντα ρει'– everything flows? *Journal of Non-Newtonian Fluid Mechanics*, **81**, 133–178.

96 Barnes, H.A., Hutton, J.F., and Walters, K. (1989) *An Introduction to Rheology*, Elsevier, Amsterdam.

97 Alves, M.A., Pinho, F.T., and Oliveira, P.J. (2005) Visualizations of Boger fluid flows in a 4:1 square–square contraction. *AICHE Journal*, **51**, 2908–2922.

98 Rodd, L.E., Scott, T.P., Cooper-White, J.J., and McKinley, G.H. (2005) Capillary breakup rheometry for low viscosity elastic fluids. *Applied Rheology*, **15**, 12–27.

99 Tirtaatmadja, V. and Sridhar, T. (1993) A filament stretching device for measurement of extensional viscosity. *Journal of Rheology*, **37**, 1081–1102.

100 McKinley, G.H. and Sridhar, T. (2002) Filament-stretching rheometry of complex fluids. *Annual Review of Fluid Mechanics*, **34**, 375–415.

101 Sentmanat, M.L. (2003) A novel device for characterizing polymer flows in uniaxial extension. SPE, ANTEC Proceedings, pp. 992–996.

102 Lielens, G., Keunings, R., and Legat, V. (1999) The FENE-L and FENE-LS closure approximations to the kinetic theory of finitely extensible dumbbells. *Journal of Non-Newtonian Fluid Mechanics*, **87**, 179–196.

103 Tanner, R.I. (2000) *Engineeering Rheology*, 2nd edn, Oxford Eng. Science Series 52, Oxford University Press, New York.

104 Ewoldt, R.H., Hosoi, A.E., and McKinley, G.H. (2008) New measures for characterizing nonlinear viscoelasticity in large amplitude oscillatory shear. *Journal of Rheology*, **35** (4), 647–685.

105 Beris, A.N. and Edwards, B.J. (1994) *Thermodynamics of Flowing Systems, Oxford Engineering Science Series 36*, Oxford Science Publications, New York.

106 Wapperom, P. (1995) Nonisothermal flows of viscoelastic fluids. Thermodynamics, analysis and numerics. PhD thesis. Technical University of Delft, Holland.

107 Wapperom, P. and Hulsen, M.A. (1998) Thermodynamics of viscoelastic fluids: the temperature equation. *Journal of Rheology*, **42**, 999–1019.

108 Nóbrega, J.M., Pinho, F.T., Oliveira, P.J., and Carneiro, O.S. (2004) Accounting for temperature-dependent properties in viscoelastic duct flows. *International Journal of Heat and Mass Transfer*, **47**, 1141–1158.

109 Bird, R.B., Armstrong, R.C., and Hassager, O. (1987) *Dynamics of Polymeric Liquids. Volume 2: Kinetic Theory*, Wiley, New York.

110 Bird, R.B., Stewart, W.E., and Lightfoot, E.N. (2002) *Transport Phenomena*, 2nd edn, John Wiley & Sons Inc., New York.

111 Astarita, G. and Marrucci, G. (1974) *Principles of Non-Newtonian Fluid Mechanics*, McGraw-Hill, London, New York.

112 Ferry, J.D. (1981) *Viscoelastic Properties of Polymers*, 2nd edn, John Wiley, New York.

113 Wapperom, P., Hulsen, M.A., and van der Zanden, J.P.P.M. (1998) A numerical method for steady and nonisothermal viscoelastic fluid flow for high Deborah and Péclet numbers. *Rheologica Acta*, **37**, 73–88.

114 Chilcott, M.D. and Rallison, J.M. (1988) Creeping flow of dilute polymer solutions past cylinders and spheres. *Journal of Non-Newtonian Fluid Mechanics*, **29**, 381–432.

115 Stokes, J.R., Graham, L.J.W., Lawson, N.J., and Boger, D.V. (2001) Swirling flow of viscoelastic fluids. Part 2: Elastic effects. *Journal of Fluid Mechanics*, **429**, 117–153.

116 Larson, R.G. (1988) *Constitutive Equations for Polymer Melts and Solutions*, Butterworths, Boston.

117 Huilgol, R.R. and Phan-Thien, N. (1997) *Fluid Mechanics of Viscoelasticity*, Elsevier, Amsterdam.

118 Dhinakaran, S., Afonso, A.M., Alves, M.A., and Pinho, F.T. (2010) Steady viscoelastic fluid flow in microchannels under electrokinetic forces: PTT model. *Journal of Colloid and Interface Science*, **344**, 513–520.

119 Bird, R.B. and Curtiss, C.F. (1998) Thermoviscoelasticity: continuum-molecular connections. *Journal of Non-Newtonian Fluid Mechanics*, **79**, 255–259.

120 Peters, G.W.M. and Baaijens, F.P.T. (1997) Modelling of non-isothermal viscoelastic flows. *Journal of Non-Newtonian Fluid Mechanics*, **68**, 205–224.

121 Larson, R.G., Shaqfeh, E.S.G., and Muller, S.J. (1990) A purely elastic instability in Taylor–Couette flow. *Journal of Fluid Mechanics*, **218**, 573–600.

122 McKinley, G.H., Pakdel, P., and Öztekin, A. (1996) Rheological and geometric scaling of purely elastic flow instabilities. *Journal of Non-Newtonian Fluid Mechanics*, **67**, 19–47.

123 Shaqfeh, E.S.G. (1996) Purely elastic instabilities in viscometric flows. *Annual Review of Fluid Mechanics*, **28**, 129–185.

124 Pakdel, P. and McKinley, G.H. (1998) Cavity flows of elastic liquids: Purely elastic instabilities. *Physics of Fluids*, **10**, 1058–1070.

125 Alves, M.A. and Poole, R.J. (2007) Divergent flow in contractions. *Journal of Non-Newtonian Fluid Mechanics*, **144**, 140–148.

126 Boger, D.V. (1987) Viscoelastic flows through contractions. *Annual Review of Fluid Mechanics*, **19**, 157–182.

127 Owens, R.G. and Phillips, T.N. (2002) *Computational Rheology*, Imperial College Press, London.

128 Evans, R.E. and Walters, K. (1986) Flow characteristics associated with abrupt changes in geometry in the case of highly elastic liquids. *Journal of Non-Newtonian Fluid Mechanics*, **20**, 11–29.

129 Evans, R.E. and Walters, K. (1989) Further remarks on the lip-vortex mechanism of vortex enhancement in planar-contraction flows. *Journal of Non-Newtonian Fluid Mechanics*, **32**, 95–105.

130 Rothstein, J.P. and McKinley, G.H. (1999) Extensional flow of a polystyrene Boger fluid through a 4:1:4 axisymmetric contraction-expansion. *Journal of Non-Newtonian Fluid Mechanics*, **86**, 61–88.

131 Boger, D.V., Hur, D.U., and Binnington, R.J. (1986) Further observations of elastic effects in tubular entry flows. *Journal of Non-Newtonian Fluid Mechanics*, **20**, 31–49.

132 Alves, M.A., Oliveira, P.J., and Pinho, F.T. (2004) On the effect of contraction ratio in viscoelastic flow through abrupt contractions. *Journal of Non-Newtonian Fluid Mechanics*, **122**, 117–130.

133 Oliveira, M.S.N., Pinho, F.T., Oliveira, P.J., and Alves, M.A. (2007) Effect of contraction ratio upon viscoelastic flow in contractions: The axisymmetric case. *Journal of Non-Newtonian Fluid Mechanics*, **47**, 92–108.

134 Hassager, O. (1988) Working group on numerical techniques. in: Proceedings of the Vth Workshop on numerical methods in non-Newtonian flow. *Journal of Non-Newtonian Fluid Mechanics*, **29**, 2–5.

135 Alves, M.A., Oliveira, P.J., and Pinho, F.T. (2003) Benchmark solutions for the flow of Oldroyd-B and PTT fluids in planar contractions. *Journal of Non-Newtonian Fluid Mechanics*, **110**, 45–75.

136 Walters, K. and Webster, M.F. (2003) The distinctive CFD challenges of

computational rheology. *International Journal for Numerical Methods in Fluids*, **43**, 577–596.

137 Kim, J.M., Kim, C., Kim, J.H., Chung, C., Ahn, K.H., and Lee, S.J. (2005) High-resolution finite element simulation of 4:1 planar contraction flow of viscoelastic fluid. *Journal of Non-Newtonian Fluid Mechanics*, **129**, 23–37.

Q1 **138** Afonso, A., Oliveira, P.J., Pinho, F.T., and Alves, M.A. (2011) Dynamics of high Deborah number entry flows: A numerical study. *Journal of Fluid Mechanics*, ~~in press~~.

139 Rodd, L.E., Cooper-White, J.J., McKinley, G.H., and Boger, D.V. (2007) Role of the elasticity number in entry flow of dilute polymer solutions in microfabricated contraction geometries. *Journal of Non-Newtonian Fluid Mechanics*, **143**, 170–191.

140 Gan, H.Y., Lam, Y.C., Nguyen, N.T., Tam, K.C., and Yang, C. (2007) Efficient mixing of viscoelastic fluids in a microchannel at low Reynolds number. *Microfluid Nanofluid*, **3**, 101–108.

141 Lam, Y.C., Gan, H.Y., Nguyen, N.T., and Lie, H. (2009) Micromixer based on viscoelastic flow instability at low Reynolds number. *Biomicrofluidics*, **3**, 014106.

142 Lam, Y.C., Gan, H.Y., Nguyen, N.T., Yang, C., and Tam, K.C. (2008) Methods and apparatus for microfluidic mixing, US Patent, 2008/0259720.

143 Hemminger, O.L., Boukany, P.E., Wang, S.-Q-., and Lee, L.J. (2010) Flow pattern and molecular visualization of DNA solutions through a 4:1 planar micro-contraction. *Journal of Non-Newtonian Fluid Mechanics*, **165**, 1613–1624.

144 Perkins, T.T., Smith, D.E., Larson, R.G., and Chu, S. (1995) Stretching of a single tethered polymer in a uniform flow. *Science*, **268**, 83–87.

145 Perkins, T.T., Smith, D.E., and Chu, S. (1997) Single polymer dynamics in an elongational flow. *Science*, **276**, 2016–2021.

146 Teclemariam, N.P., Beck, V.A., Shaqfeh, E.S.G., and Muller, S.J. (2007) Dynamics of DNA polymers in post arrays: Comparison of single molecule experiments and simulations. *Macromolecules*, **40**, 3848–3859.

147 Arratia, P.E., Thomas, C.C., Diorio, J., and Gollub, J.P. (2006) Elastic instabilities of polymer solutions in cross-channel flow. *Physical Review Letters*, **96**, 144502-1–144502-4.

148 Poole, R.J., Alves, M.A., and Oliveira, P.J. (2007) Purely-elastic flow asymmetries. *Physical Review Letters*, **99**, 164503.

149 Afonso, A.M., Alves, M.A., Poole, R.J., Oliveira, P.J., and Pinho, F.T. (2011) Viscoelastic flows in mixing-separating cells. *Journal of Engineering Mathematics*. In press. doi: 10.1007/s10665-010-9384-x Q2

150 Afonso, A.M., Alves, M.A., and Pinho, F.T. (2010) Purely-elastic flow instabilities in a 3D six arms cross slot geometry. *Journal of Non-Newtonian Fluid Mechanics*, **165**, 743–751.

151 Mompean, G., Thompson, R.L., and Mendes, P.R.S. (2003) A general transformation procedure for differential viscoelastic models. *Journal of Non-Newtonian Fluid Mechanics*, **111**, 151–174.

152 Schiamberg, B.A., Shereda, L.T., Hu, H., and Larson, R.G. (2006) Transitional pathway to elastic turbulence in torsional, parallel-plate flow of a polymer solution. *Journal of Fluid Mechanics*, **554**, 191–216.

153 Li, F.-C., Kinoshita, H., Li, X.-B., Oishi, M., Fujii, T., and Oshima, M. (2010) Creation of very-low-Reynolds-number chaotic fluid motions in microchannels using viscoelastic surfactant solutions. *Experimental Thermal and Fluid Science*, **34**, 20–27.

154 Burghelea, T., Segre, E., and Steinberg, V. (2007) Elastic turbulence in von Karman swirling flow between two disks. *Physics of Fluids*, **19**, 053104.

155 Fouxon, A. and Lebedev, V. (2007) Spectra of turbulence in dilute polymer solutions. *Physics of Fluids*, **15**, 2060–2072.

156 Fardin, M.A., Lopez, D., Croso, J., Grégoire, G., Cardoso, O., McKinley, G.H., and Lerouge, S. (2010) Elastic turbulence in shear banding wormlike micelles. *Physical Review Letters*, **104**, 178303.

157 Morozov, A.N. and van Saarloos, W. (2007) An introductory essay on subcritical instabilities and the transition to turbulence in viscoelastic parallel shear flows. *Psychological Reports*, **447**, 112–143.

158 Bistagnino, A., Boffetta, G., Celani, A., Mazzino, A., Puliafito, A., and Vergassola, M. (2007) Nonlinear dynamics of the viscoelastic Kolmogorov flow. *Journal of Fluid Mechanics*, **590**, 61–80.

159 Berti, S. and Boffetta, G. (2010) Elastic waves and transition to elastic turbulence in a two-dimensional viscoelastic Kolmogorov flow. *Physical Review E*, **82**, 036314.

160 Pennathur, S. (2008) Flow control in microfluidics: Are the workhorse flows adequate? *Lab on a Chip*, **8**, 383–387.

161 Li, D. (ed.) (2008) *Encyclopedia of Microfluidic and Nanofluidic*, Springe, Berlin.

162 Afonso, A.M., Alves, M.A., and Pinho, F.T. (2009) Analytical solution of mixed electro-osmotic/pressure driven flows of viscoelastic fluids in microchannels. *Journal of Non-Newtonian Fluid Mechanics*, **159**, 50–63.

163 Lin, H., Storey, B.D., Oddy, M.H., Chen, C.H., and Santiago, J.G. (2004) Instability of electrokinetic microchannel flows with conductivity gradients. *Physics of Fluids*, **16**, 1922–1935.

164 Chen, C.-H., Lin, H., Lele, S.K., and Santiago, J.G. (2005) Convective and absolute electrokinetic instability with conductivity gradients. *Journal of Fluid Mechanics*, **524**, 263–303.

165 Shin, S.M., Kang, I.S., and Cho, Y.-K. (2005) Mixing enhancement by using electrokinetic instability under time-periodic electric field. *Journal of Micromechanics and Microengineering*, **15**, 455–462.

166 Chang, C.-C. and Yang, R.-J. (2009) Chaotic mixing in electro-osmotic flows driven by spatiotemporal surface charge modulation. *Physics of Fluids*, **21**, 052004.

167 Bazant, M.Z. and Squires, T.M. (2010) Induced-charge electrokinetic phenomena. *Current Opinion in Colloid and Interface Science*, **15**, 203–213.

168 Das, S. and Chakraborty, S. (2006) Analytical solutions for velocity, temperature and concentration distribution in electroosmotic microchannel flows of a non-Newtonian bio-fluid. *Analytica Chimica Acta*, **559**, 15–24.

169 Chakraborty, S. (2007) Electroosmotically driven capillary transport of typical non-Newtonian biofluids in rectangular microchannels. *Analytica Chimica Acta*, **605**, 175–184.

170 Berli, C.L.A. and Olivares, M.L. (2008) Electrokinetic flow of non-Newtonian fluids in microchannels. *Journal of Colloid and Interface Science*, **320**, 582–589.

171 Park, H.M. and Lee, W.M. (2008) Helmholtz-Smoluchowski velocity for viscoelastic electroosmotic flows. *Journal of Colloid and Interface Science*, **317**, 631–636.

172 Afonso, A.M., Alves, M.A., and Pinho, F.T. (2011) Electro-osmotic flow of viscoelastic fluids in microchannels under asymmetric zeta potentials. *Journal of Engineering Mathematics*. In Press. doi: 10.1007/s10665-010-9421-9 Q3

173 Sousa, J.J., Afonso, A.M., Pinho, F.T., and Alves, M.A. (2011) Effect of the skimming layer on electro-osmotic-Poiseuille flows of viscoelastic fluids. *Microfluid Nanofluid*, **10**, 107–122.

174 Bello, M.S., De Besi, P., Rezzonico, R., Righetti, P.G., and Casiraghi, E. (1994) Electroosmosis of polymer solutions in fused silica capillaries. *Electrophoresis*, **15**, 623–626.

175 Baumler, H., Neu, B., Iovtchev, S., Budde, A., Kiesewetter, H., Latza, R., and Donath, E. (1999) Electroosmosis and polymer depletion layers near surface conducting particles are detectable by low frequency electrorotation. *Colloids and Surfaces A*, **149**, 389–396.

176 Chang, F.-M. and Tsao, H.-K. (2007) Drag reduction in electro-osmosis of polymer solutions. *Applied Physics Letters*, **90**, 194105.

177 Bryce, R.M. and Freeman, M.R. (2010) Abatement of mixing in shear-free elongationally unstable viscoelastic microflows. *Lab on a Chip*, **10**, 1436–1441.

178 Bryce, R.M. and Freeman, M.R. (2010) Extensional instability in electro-osmotic microflows of polymer solutions. *Physical Review E*, **81**, 036328.

179 Graham, R.S. and McLeish, T.C.B. (2008) Emerging applications for models of molecular rheology. *Journal of Non-Newtonian Fluid Mechanics*, **150**, 11–18.

180 Hsieh, C.-C. and Doyle, P.S. (2008) Studying confined polymers using single-molecule DNA experiments. *Korea-Australia Rheology Journal*, **20**, 127–142.

181 Larson, R.G. (2007) Going with the flow. *Science*, **318**, 57–58.

182 Wu, D., Qin, J., and Lin, B. (2008) Electrophoretic separations on microfluidic chips. *Journal of Chromatography. A*, **1184**, 542–559.

183 Kim, J.M. and Doyle, P.S. (2007) Design and numerical simulation of a DNA electrophoretic stretching device. *Lab on a Chip*, **7**, 213–225.

184 Juang, Y.-J., Wang, S., Hu, X., and Lee, L.J. (2004) Dynamics of single polymers in a stagnation flow induced by electrokinetics. *Physical Review Letters*, **93**, 268105.

185 Balducci, A. and Doyle, P.S. (2008) Conformational preconditioning by electrophoresis of DNA through a finite obstacle array. *Macromolecules*, **41**, 5485–5492.

186 Tang, J. and Doyle, P.S. (2007) Electrophoretic stretching of DNA molecules using microscale T junctions. *Applied Physics Letters*, **90**, 224103.

187 Perkins, T.T., Quake, S.R., Smith, D.E., and Chu, S. (1994) Relaxation of a single DNA molecule observed by optical microscopy. *Science*, **264**, 822–826.

188 Ferree, S. and Blanch, H.W. (2004) The hydrodynamics of DNA electrophoretic stretch and relaxation in a polymer solution. *Biophysical Journal*, **87**, 468–475.

189 Liu, Y., Jun, Y., and Steinberg, V. (2007) Longest relaxation times of double-stranded and single-stranded DNA. *Macromolecules*, **40**, 2172–2176.

Keywords/Abstract

Dear Author,

Keywords and abstracts will not be included in the print version of your chapter but only in the online version.

Please check and/or supply keywords. If you supplied an abstract with the manuscript, please check the typeset version.

If you did not provide an abstract, the section headings will be displayed instead of an abstract text in the online version.

Abstract

Viscoelastic fluids possess nonlinear rheological behavior that drives flow instabilities at the low Reynolds numbers typically found at the microscale. These elastic-driven instabilities are linked to the presence of large normal stresses and streamline curvature, and appear at critical Weissenberg numbers in a wide range of flows, either dominated by shear, by extension, or having mixed kinematics. The Weissenberg number is a dimensionless number inversely proportional to a characteristic length scale of the flow. Therefore, elastic instabilities are easily present in microfluidic flows, where they constitute a useful passive mixing mechanism that in the limit of very high Weissenberg numbers can exist in the form of elastic turbulence. In this chapter, we report and discuss microfluidic flows of complex fluids and elastic-driven instabilities in a large set of flow geometries. We also present an overview of the relevance of microfluidic systems operating with viscoelastic fluids and describe the main rheological material properties and the governing equations for pressure-gradient and electro-osmotic driven non-Newtonian fluid flows.

Keywords: viscoelastic fluids; microfluidic systems; Reynolds number; Newtonian fluids; Couette flow; Weissenberg effect; ~~small amplitude oscillatory shear (SAOS)~~.

Author Query

1. Please update Ref. [138].
2. Please update Ref. [149].
3. Please update Ref. [172].